BL1B

Two-Photon Spectroscopy of Core Excitons with the Combinational Use of Synchrotron Radiation and Laser Light

T. Tsujibayashi[1], J. Azuma[2], M. Watanabe[3], O. Arimoto[4], M. Itoh[5], S. Nakanishi[6], H. Itoh[6], M. Kamada[2]

[1]*Department of Physics, Osaka Dental Univ., Hirakata 573-1121, Japan*
[2]*Synchrotron Light Application Center, Saga Univ., Saga 840-8502, Japan*
[3]*Department of Interdisciplinary Environment, Kyoto Univ., Kyoto 606-8501, Japan*
[4]*Department of Physics, Okayama Univ., Okayama 700-8530, Japan*
[5]*Department of Electrical & Electronic Engineering, Shinshu Univ., Nagano 380-8553, Japan*
[6]*Department of Advanced Materials Science, Kagawa Univ., Takamatsu 761-0396, Japan*

Synchrotron radiation facilities and lasers are the most valuable scientific inventions of the 20th century. We have constructed a system for a combinational use of both the light sources at BL1B [1, 2] and applied it to the study of valence excitons of wide bandgap materials [3]. Furthermore, we performed two-photon excitation of core excitons in BaF_2, and the results of the experiments were published recently [4, 5]. In this paper, we present the summary of those works.

The combinational use of synchrotron radiation (SR) and laser light dates back to 1980s. N_2 and Nd:YAG lasers with repetition rates lower than 100 Hz were used in the early stages of experiments [6, 7]. For the purpose of efficient measurements, it is desirable that the laser pulses are synchronized completely with SR pulses. The development of a mode-locked laser enabled such experiments.

The aim of our two-photon absorption (TPA) measurement is to investigate unoccupied states in solids. The TPA is a powerful technique as well as inverse-photoemission measurement since its final state of the transition is restricted by the selection rules. In order to specify the final states, core electron excitation are advantageous to valence electron excitation, since core states are often flat in the *k*-space and have well-defined symmetry. The TPA is suitable for the measurement of high-angular momentum states such as *d* and *f* orbitals because these states cannot be reached by dipole transitions from many core states, which consist of *s* and *p* orbitals.

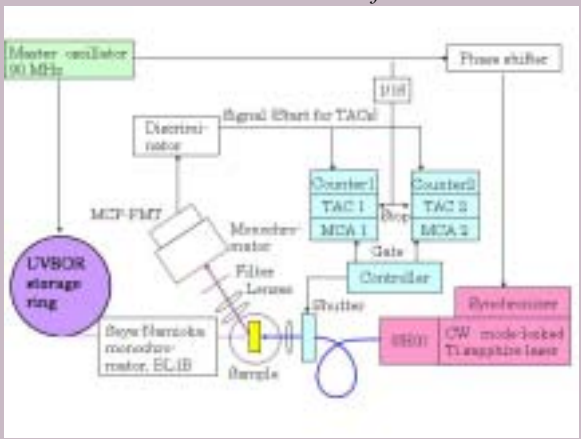

Fig. 1 The experimental setup of two-photon excitation with use of SR and laser. Luminescence from the sample is detected as the signal.

We show the experimental setup in Fig. 1. The laser pulses are synchronized with SR pulses through electronic devices. The laser light propagates through an optical fiber to the port of measurement. We detected luminescence of the sample with use of a photomultiplier of the microchannel plate-type through the time-correlated single photon counting method. The laser light was turned on and off using an optical shutter. The output of the detector is accumulated in two MCAs: one works when the laser light is on and the other when the light is off. The difference is attributed to the signal due to TPA.

Figure 2 shows the TPA spectrum of BaF_2. The spin-orbit splittings of 4*f* and 6*p* states of Ba ions in BaF_2 were found to be 0.7 and 1.4 eV, respectively [4]. These values are well explained by the relativistic quantum theory. It tells that the spin-orbit splittings of hydrogen-like orbits specified (n, l) have the following expression,

$$\Delta_{n,l} \propto \left(n^3 l(l+1)\right)^{-1}. \quad (1)$$

Expression (1) gives relative values of the splittings:

$$\Delta_{5p} : \Delta_{5d} : \Delta_{4f} : \Delta_{6p} \approx 3.0 : 1.0 : 1.0 : 1.7. \quad (2)$$

Since the splitting of 5*p* levels was obtained experimentally to be 2.2 eV [8], those of the other states are calculated with use of Eq. (2).

The calculated splitting of 5*d* states raises a query about the so far proposed interpretations of the reflectivity spectrum of 5*d*-core excitons in BaF_2. The

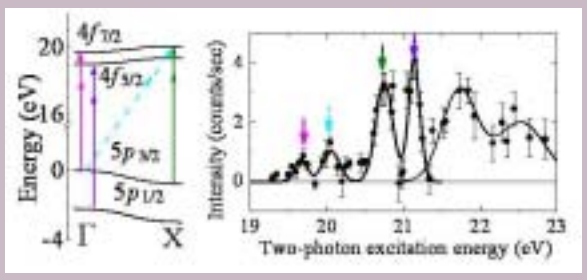

Fig. 2 The TPA spectrum of 4*f*- and 6*p*-core excitons in BaF_2. The energy diagram of 4*f* levels is depicted on the left. See Ref. 4 for the details.

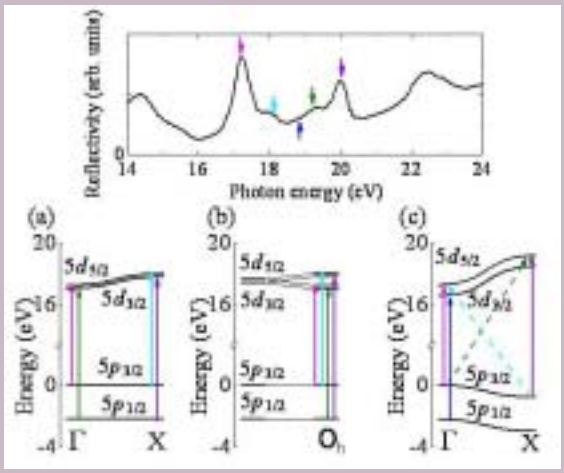

Fig. 3 Which is the true diagram? Schematic energy diagrams of 5*d* core excitons in BaF_2 based on different models are shown. The upper panel shows the reflectivity spectrum of the excitons. The 5*p* and 5*d* levels split due to spin-orbit interaction. The $p_{1/2}$-$d_{3/2}$ and $p_{3/2}$-$d_{5/2}$ transitions are allowed in electric dipole transitions. The origin of the multi peaks is attributed to the dispersion of the levels in (a) and (c), whereas to the crystal field effect in (b). The exciton binding energy is assumed to be constant and included in the diagrams above.

first precise measurement of the spectrum of BaF_2 in the core excitation region was reported in 1972 [9], and the interpretation of the peaks is schematically depicted in Fig. 3 (a). The splitting of 5*d* levels is obtained to be 0.2 eV. An alternative interpretation of the spectrum is possible [10]. Figure 3 (b) is based on a model where the crystal field splitting is assumed to be as large as 0.8 eV and dispersion of the states are not taken into consideration. The splitting of 5*d* levels is deduced to be the same as the former case, which value is inconsistent with Eq. (2).

The diagram of Fig. 3 (c) is based on a recent band calculation of energy levels [11]. It gives an interpretation consistent with Eq. (2).

Spectroscopic study of core excitons revealed the conduction band structure as described above. Besides static properties, dynamical behavior of core excitons was measured through the system depicted in Fig. 1. An example of temporal behavior of the signal luminescence is shown in Fig. 4. The lifetime of the two-photon excited 6*p*-exciton was obtained to be 0.2 ns [5].

The time resolution of the system is mainly determined by excitation pulse widths. As depicted in the upper panel of Fig. 4, the pulse width of SR was about 0.6 ns (under the single bunch operation), and that of the laser was 0.3 ns. The laser pulse expanded during the propagation through the 50-m long fiber. The laser pulse width can be shortened by shortening the length of the fiber. However, it should be noted that the shorter the pulse width is, the smaller the overlap with the SR pulse is. Consequently, the signal

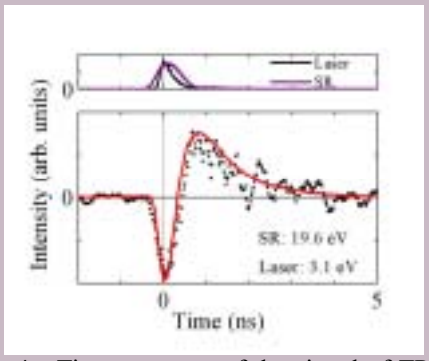

Fig. 4 Time-response of the signal of TPA. The output of the detector under excitation exclusively with SR is subtracted from that with both the SR and laser. The photon energy of SR is enough to excite a core electron to a 5*d* level. The dip can be interpreted that two-photon excited core excitons have a finite lifetime, which should be compared to the fast recombination of one-photon excited core electron. See Ref. 5 for the details.

becomes weaker. In order to secure sufficient intensity of the signal, the use of an undulator beamline may be indispensable, though sample damage should be carefully avoided.

In the present measuring system, TPA is detected by luminescence. Unfortunately, TPA is not always accompanied by characteristic luminescence, such as Auger-free luminescence of BaF_2 and other materials [12]. In order to study wide range of materials, a new technique that does not need such luminescence should be developed. Detecting reflectivity change might be a powerful technique in the future.

[1] T. Tsujibayashi *et al.*, UVSOR Activity Report 1996 (1997) 52.
[2] S. Asaka *et al.*, Rev. Sci. Instrum. **69** (1998) 1931.
[3] T. Tsujibayashi *et al.*, Phys. Rev. B **60** (1999) R8442
[4] T. Tsujibayashi *et al.*, Phys. Rev. Lett. **94** (2005) 076401.
[5] T. Tsujibayashi *et al.*, phys. stat. sol. (c) **2** (2005) 228.
[6] V. Saile *et al.*, Phys. Lett. **79A** (1980) 221.
[7] R. Pizzoferrato *et al.*, Europhys. Lett. **2** (1986) 571.
[8] J. Reader and G.L. Epstein, J. Opt. Soc. Am. **65** (1975) 638.
[9] G.W. Rubloff, Phys. Rev. B **5** (1972) 662.
[10] M. Yuri *et al.*, J Phys. Soc. Jpn. **61** (1992) 2557.
[11] H. Jiang *et al.*, J. Phys. Condens. Matter **15** (2003) 709.
[12] M. Itoh, *Recent Research Developments in Physics Vol.4* (Transworld Research Network, Trivanduram, 2003) Chap. 11.

BL1A, 5B, 7B&8B1

Time Resolved Decay Curves of AlGaN and InAlGaN Measured in the Wide Energy Range

S. Naoe[1], S. Hamada[2], K. Fukui[2], H. Hirayama[3], H. Miyake[4], K. Hiramatsu[4]
[1]*Faculty of Engineering, Kanazawa University, Ishikawa 920-1192, Japan*
[2]*Research Center for Development of Far-Infrared Region, Fukui 910-8507, Japan*
[3]*The Institute of Physical and Chemical Research, Wako 351-0198, Japan*
[4]*Faculty of Engineering, Mie University, Mie 514-8507, Japan*

AlGaN is the promising optical material having variable band gap energy by selecting a compositional rate of the elements. However, the intensity of emission in AlGaN loses rapidly its intensity with increasing temperature, though InAlGaN gives effective luminescence intensity at RT. The emission bands of those two alloy systems are basically similar. Both of them consist of two photoluminescence (PL) bands. One is B-band emission which is ultraviolet (UV) emission band due to exciton, and the other is visible (VIS) emission band caused by some defects or impurities (Y-band). Therefore, to investigate the precise emission process of III-V nitrides, the comparative studies of PL in between AlGaN and InAlGaN become important.

All samples are made by MOCVD (MOVPE) methods. The thickness of AlGaN thin films is about 1 μm on 1 μm AlN single crystal film with sapphire substrates and that of InAlGaN thin films is about 80 nm on SiC substrates with $Al_{0.2}Ga_{0.8}N$ buffer layers. In our study, multi-bunch mode (15 full + 1 empty bunchs, 11.1 ns period) of UVSOR is used as the usual stationary light source and single-bunch mode (177.7 ns period, ~ 0.5 ns width) as the pulse light source for time resolved measurement by using time correlated single photon counting method (TCSPC). Time resolved decay (TRD) measurements have been performed at BL7B, BL5B, BL8B1 and BL1A. Same conventional 30 cm monochromator via optical fiber is used to measure both PL spectra and TRD curves of all samples.

In our previous work, TRD results in band-to-band excitation (at BL7B) of both AlGaN and InAlGaN are analyzed by using the same model of three single exponential components linear combination model (decay time of the fast component is in less than sub-ns order, middle in ns, slow in 10 ns). The fast one is the main PL component at RT. Both middle and slow ones rapidly decrease with increasing temperature. Figs. 1 and 2 show B-band TRD curves at 26 K of $Al_{0.54}Ga_{0.46}N$ and $In_{0.05}Al_{0.20}Ga_{0.75}N$, respectively. Excitation energies are 4.7 eV (BL7B), 95 eV (BL5B), 405 eV (BL8B1) and 1.56 keV (BL1A). The fast component of InAlGaN TRD is much stronger than that of AlGaN even at low temperature. This is one of the reasons that InAlGaN is used as the active layer in UV-LED operated at RT. In the inner shell excitation, many electron–hole pairs are produced during the decay process of core hole coming up to valence band (photon multiplication), and make recombination as both B- and Y-band PL. The behavior of three components of TRD in the inner shell excitation becomes the interesting study to analyze the emission mechanisms in AlGaN. A rate of the fast component becomes to increase with increasing the excitation photon energy and to take the resembling curve to that of InAlGaN gradually. This result suggests one possible model that the optical transition corresponding to the fast component in AlGaN may be caused by direct overlap of the wave function between electron and hole states. The overlap of wave functions will occur in the situation of many electron-hole pairs gathering at the band edge. On the other hand, the fast component in InAlGaN will be caused by the mixing of the allowed part of wave function by the effect of incorporation of In elements.

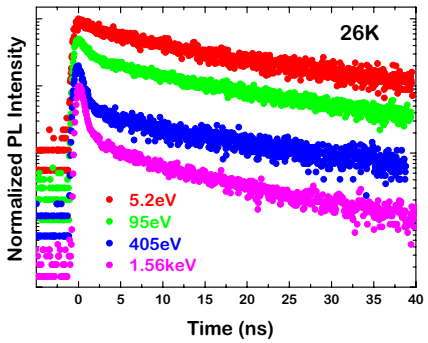

Fig. 1 Time resolved decay curves of $Al_{0.54}Ga_{0.46}N$ at various excitation energies. Each spectrum is shifted vertically for convenience.

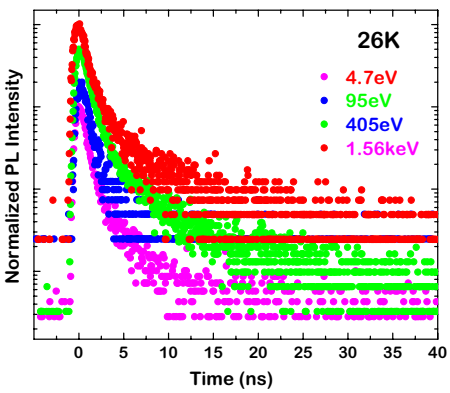

Fig. 2 Time resolved decay curves of $In_{0.05}Al_{0.20}Ga_{0.75}N$ at various excitation energies. Each spectrum is shifted vertically for convenience.

BL1A

XAFS Study on Silica Glasses Irradiated in Nuclear Reactor

T. Yoshida[1], T. Tanabe[1], H. Yoshida[2]

[1]*Department of Materials, Physics and Energy Engineering, Nagoya University, Furo-cho, Chikusa-ku, Nagoya 464-8603, Japan*

[2]*Department of Applied Chemistry, Graduate School of Engineering, Nagoya University, Nagoya 464-8603, Japan*

Irradiation effects by high-energy particles such as neutron and ions on silica glasses are one of the main concerns for their application as optical windows, insulators and optical fibers in nuclear environments. The chemical states and density of defects in silica glasses should be closely related to their optical and physical properties such as the transparency and hardness. However, it is still difficult to observe the structures of the defects at an atomic scale in a SiO_2 glass, because the structural changes in its amorphous nature does not allow us to apply diffraction techniques. In the present work, we have investigated the change of the local structure of the SiO_2 glass before and after in-reactor (*i.e.*, neutron and γ-ray) irradiation by Si K-edge X-ray absorption fine structure.

Samples used in this work were a synthesized silica glass (T-4040) of 13 mm diameter and 2 mm thickness with OH content of 800 ppm. The samples were irradiated in the nuclear reactor YAYOI at the University of Tokyo. YAYOI was operated with a power of 1.5 kW, where a neutron flux was about $6x10^{11}$ n/m^{2}s with an average neutron energy of 1.3 MeV and γ ray level was about 3.0 kGy/h.

Si K-edge X-ray absorption spectra were recorded under vacuum (<10^{-6} Pa) at room temperature at BL7A and 1A station of UVSOR, or at BL11B station of Photon Factory, Institute of Materials Structure Science, High Energy Accelerator Research Organization (KEK-PF), using a two-crystal InSb(111) monochromator. Two different recording modes, *i.e.* a total electron yield (TEY) mode and a fluorescent X-ray yield (FY) mode were employed with detectors consisting of an electron multiplier and a gas-flow proportional counter, respectively.

Fig. 1 compares the radial structure functions (RSFs) obtained from Fourier transforms of the k-weighted Si K-edge EXAFS spectra of a synthesized silica glass before and after in-reactor irradiation together with that of a SiO_2 crystal (quartz) sample as a reference. We also performed curve-fitting analysis of the Fourier-filtered EXAFS by the least-squares method. In Fig. 1, the peaks in the region of 0.8-3.2 Å were isolated with a Hanning window, and inversely Fourier transformed. The curve-fitting analysis was carried out with Si-O and Si-Si shells. The curve-fitting results are summarized in Table 1.

The EXAFS spectra of the silica glasses irradiated with the low neutron fluence (less than ca. 1 x 10^{19} n/m^2) were fundamentally the same as those of their unirradiated ones (not shown here). The structural change was recognized in the EXAFS spectra of the silica glasses irradiated with more than 2 x 10^{19} n/m^2. In the RSFs, it should be noted that the peak intensity at 1.2 Å due to the Si-O bond increased to a level similar to that of the quartz crystal. Moreover, the coordination numbers of the first neighboring oxygen atoms increased from ca. 3.7 to ca. 4.3 after in-reactor irradiation (see Table 1). At the same time the coordination number of the second neighboring Si atoms decreased, *i.e.*, the Fourier-filtered EXAFS spectra of the irradiated silica glasses were not fitted well using a Si-Si shell. However, the curve-fitting using a Si-O shell instead of Si-Si shell was successful. The distance 2.92 Å thus evaluated corresponds to the path length of the multiple scattering for Si-O-O in the regular SiO_4 tetrahedron. These results suggest some decoupling of neighboring distorted SiO_4 tetrahedrons in a silica glass via the atomic displacement by neutron irradiation. Accordingly, the decoupled distorted SiO_4 tetrahedrons could be relaxed and return to regular or isolated SiO_4 tetrahedron and the O-Si-O angles would be more uniform after the irradiation, as observed in the growth of the peak assigned to Si-O in RSFs. This does not mean the recovery of long range orders (or recrystallization). The irradiation certainly gave more disorder in long range as the appearance of Si precipitates or each tetrahedron became more isolated.

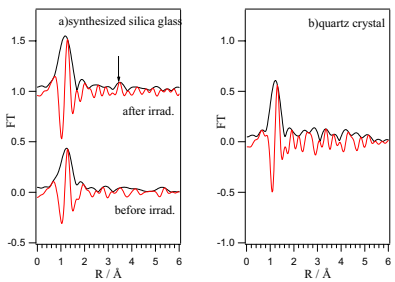

Fig. 1 Radial structural functions of k-weighted Si K-edge EXAFS spectra of (a) the synthesized silica glass before and after in-reactor irradiation, and (b) a quartz crystal. The neutron fluence of the irradiated synthesized silica glass is 2.7 x 10^{20} n/m^2.

Table 1 Results of curve-fitting analyses

Sample	Shell	coordination number	interatomic distance(Å)	$\Delta\sigma^{2\,a)}$ (Å^2)
Quartz	Si-O	4.0	1.61	0
	Si-Si	4.0	3.02	0.00285
Syn.silica (unirradiated)	Si-O	3.7	1.61	0.00269
	Si-Si	0.8	3.09	0.00332
Irrad. syn. silica (2.7x10^{20} n/m^2)	Si-O	4.3	1.60	0.00114
	Si-O	1.5	2.91	0.00150
	Si-Si[b)]	2.0	3.86	-0.00358

BL1B

Two-Molecule Absorptions of Oxygen under High Pressure

Y. Akahama, T. Moriwaki, H. Kawamura
Department of Material Science, Graduate School of Material Science, 3-2-1 Kouto, Kamigohri, Hyogo 678-1297 Japan

Introduction

The properties of condensed molecular oxygen have been of considerable interest for many years because of its simple and fundamental molecular magnetism. In order to understand the properties on the base of the electronic structure of the molecule, the study of electronic spectra is indispensable. Our recent studies on UV absorption spectra of condensed oxygen up to 13 GPa have revealed that a relatively strong absorption band was observed above 5 eV in super-critical fluid, and further the new UV band constructed the valence band of the β solid phase [1]. The results suggest that the intermolecular interaction plays a main role in the optical properties. Therefore, we concentrate our attention on the high-pressure behavior of two molecule absorptions.

Experimental

Liquid oxygen was loaded in the sample chamber of a sapphire or diamond-anvil pressure cell and the pressure was regulated at 300 K based on a ruby pressure scale. The typical thickness and diameter of the sample chamber were about 150 μm and 300 μm, respectively. UV absorption measurements were carried out over a range from 0.2 to 8 GPa using an UV source at the BL1B and 7B beam lines.

Results and Discussion

Figure 1 shows the absorption spectra of condensed oxygen at pressures up to 8 GPa and at 300 K. The absorption bands are due to two-molecule transitions of $2^3\Sigma_g^- \rightarrow {}^1\Sigma_g^+ + {}^1\Delta_g$ (0-0) and $2^1\Delta_g$ (0-0, 1-0, 2-0) and the values of wavelength of these bands are consistent with those in liquid phase at ambient pressure. The absorption intensity increases with pressure in the fluid phase. The behavior of the intensity is also consistent with the previous result in a pressure range up to 35 atoms [2]. Sudden increase in the intensity is observed above solidification pressure of 5.9 GPa. The increase in the intensity, which was correlated with the behavior of the UV absorption band at 5 eV, is suggestive of the enhancement of intermolecular interaction. The relatively weak absorption of the $2^3\Sigma_g^- \rightarrow {}^1\Sigma_g^+ + {}^1\Delta_g$ (0-0) transition could not be detected in the solid phase due to a strong absorption of diamond anvils.

Figure 2 shows the pressure dependence of the wavelengths of the two-molecule absorption bands. The wavelength of the ${}^1\Sigma_g^+ + {}^1\Delta_g$ (0-0) band is independent of pressure while those of $2^1\Delta_g$ (0-0, 1-0, 2-0) bands show a blue shift. From these spectra data, we could estimate the pressure dependence of the energy of excited states ${}^1\Sigma_g^+$ and ${}^1\Delta_g$ from the ground state. As the results, the energy of ${}^1\Delta_g$ rose with increasing pressure. On the contrary, the energy of ${}^1\Sigma_g^+$ fell down. This pressure behavior of ${}^1\Sigma_g^+$ supports recent results of molecular dynamic simulations [3], in which an insulator to semi-metal transition has been suggested by overlapping between the excited state and the ground state indirectly in the momentum space.

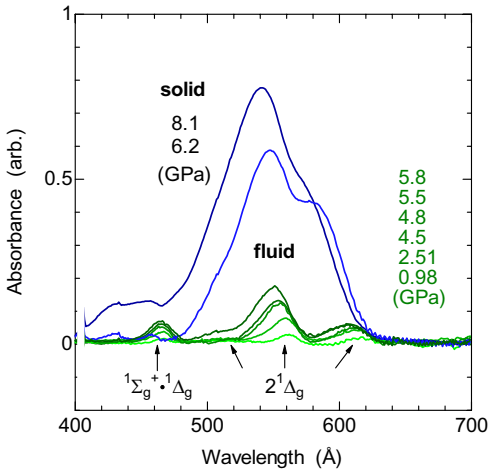

Fig. 1 Two-molecule absorption spectra at various pressure at 300 K.

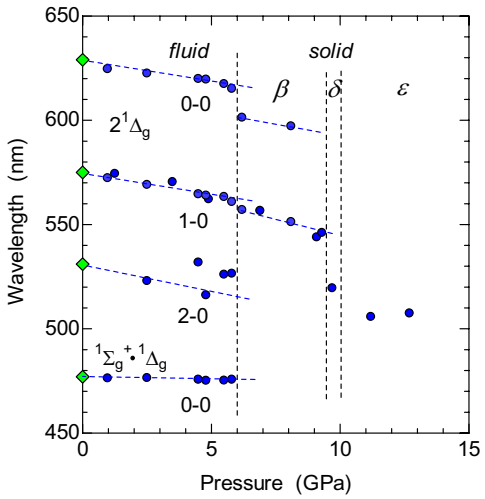

Fig. 2 Pressure dependence of the wavelengths of two-molecule absorption bands.

[1] Y. Akahama and H. Kawamura, Chem. Phys. Lett. **392** (2004) 467.
[2] V. I. Dianov-Klokov, Opt. Spectrosc. (USSR) **16** (1964) 224.
[3] S. Serra *et al.*, Phys. Rev. Lett. **80** (1998) 5160.

BL1B

VUV Reflectivity Spectra of $CaMoO_4$ and $CaWO_4$ Crystals

M. Fujita[1], S. Takagi[2], N. Fujita[2], T. Shimizu[2], M. Itoh[2]
[1]*Japan Coast Guard Academy, Wakaba, Kure 737-8512 Japan*
[2]*Department of Electrical and Electronic Engineering, Shinshu University, Nagano 380-8553 Japan*

Tungstate family such as $CaWO_4$ and $PbWO_4$ is known as an intrinsic scintillation material. Recently, molybdate crystals attract much attention in the field of astro-particle physics for the detection of weakly interacting massive particles. Although extensive studies have been reported on the luminescence properties, reliable optical constants have not been established for most of tungstate and molybdate compounds. In a recent study we measured optical anisotropy of scheelite $PbWO_4$ crystals in detail and confirmed important contribution of Pb states to the electronic structures at the band edge [1].

The present paper reports anisotropic optical properties of $CaMoO_4$ and $CaWO_4$ as typical crystals of alkaline-earth metal molybdate and tungstate with scheelite-type structure.

Experiment

Reflectivity spectra were measured for polished surfaces of $CaMoO_4$ and $CaWO_4$ single crystals, with use of the polarized light parallel to the a-axis (E//a) and c-axis (E//c). The orientation of crystal axis was determined by means of a pair of crossed polarizer.

Results and Discussion

Figure 1 shows reflectivity spectra of $CaMoO_4$ and $CaWO_4$ at 8 K. Close similarity is observed between the spectra in Fig. 1(a) and (b). The structures in Fig. 1 are calssified into three groups according to the line shape and polarization dependence. In contrast to the exciton band in $PbWO_4$ [1], the lowest band 1 in $CaMoO_4$ and $CaWO_4$ is broad. The width of the band 1 for E//a is larger than that for E//c for both materials. In the region 2, the dichroism is seen distinctly.

The energy positions of the main structures in Fig. 1 agree, as a whole, with those of previous studies [2-4], but there exists serious disagreement among their relative intensities. We confirmed the data reproducibilty by measuring the reflectivity spectra on a cleaved surface of $CaWO_4$ crystal; the obtained result was almost the same as Fig. 1(b).

According to a theoretical calculation of the electronic structures of $CaMoO_4$ and $CaWO_4$ [5], the valence band is mainly built up of the O $2p$ state and the conduction band is composed of the Mo $4d$ (W $5d$) state. The molecular orbitals at the top of the valence band and the bottom of the conduction band are of t_1 and e symmetry, respectively, in MoO_4 (WO_4) oxyanion complex of T_d symmetry. Both the t_1 and e states split into two sublevels in the S_4 symmetry of scheelite crystal. The polarization dependence of the width of the band 1 would be attributed to the splittings of the t_1 state and the e state due to the crystal-field potential of S_4 symmetry.

The structures in the region 2 are assigned to the transition from the top of the valence band to the next higher conduction band of t_2 symmetry, which is mainly made of the Mo $4d$ (W $5d$) state with some hybridization of the Ca $3d$ state.

The optical transition in the region 3 is supposed to include the excitation from the valence band to the conduction band of Ca $3d$ state.

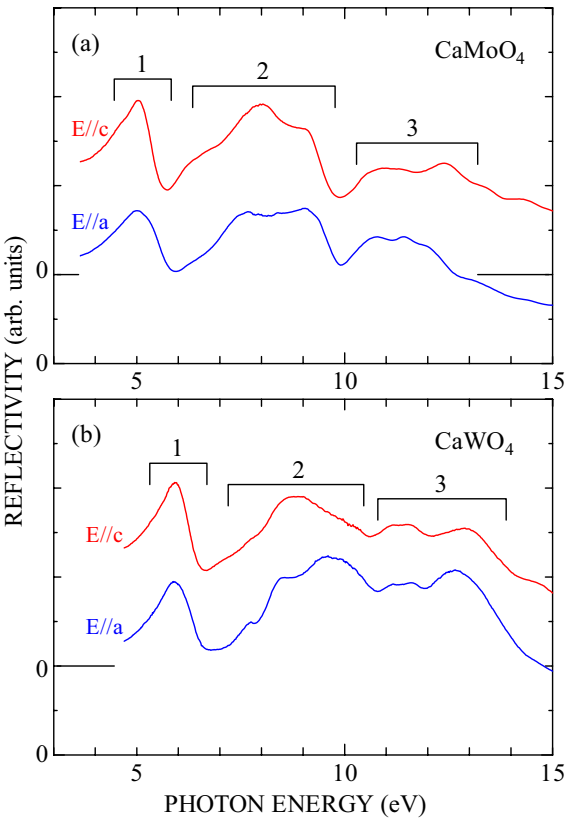

Fig. 1 Reflectivity spectra of (a) $CaMoO_4$ and (b) $CaWO_4$ at 8 K.

[1] M. Fujita *et al.*, Phys. Rev. B **65** (2002) 195105.
[2] R. Grasser *et al.*, Phys. Stat. Sol. (b) **69** (1975) 359.
[3] I. A. Kamenskikh *et al.*, Nucl. Instrum. Methods Phys. Res. A **470** (2001) 270.
[4] V. B. Mikhailik *et al.*, Phys. Stat. Sol. (b) **242** (2005) R17.
[5] Y. Zhang *et al.*, Phys. Rev. B **57** (1998) 12738.

BL1B

Characterization of Partial Discharge Degradation of Polyamide-6 Nanocomposites by a Photoluminescence Analysis

N. Fuse[1], M. Kozako[2,3], T. Tanaka[2], Y. Ohki[1]
[1]*Department of EEBS, Waseda University, Shinjuku 169-8555, Japan*
[2]*Graduate School of IPS, Waseda University, Kita-Kyushu 808-0135, Japan*
[3]*Kagoshima National College of Technology, Aira 899-5193, Japan*

Polymer nanocomposites have been attracting much attention as new materials that have high potential for wide applications. Therefore, we have been examining the dielectric properties of polyamide nanocomposites, focusing especially on their resistance against partial discharges (PDs).

Experimental

The samples investigated are polyamide-6 nanocomposite with 5 wt% mica nanofillers (NC-5) and polyamide-6 without nanofillers (PA). They are of a sheet shape 60 mm × 60 mm × 1 mm. Using the IEC (b) electrode system, which consists of a rod and a plane stainless steel electrode, ac 60-Hz high voltage was applied to the sample for 48 hours.

Using synchrotron radiation (SR) under multi-bunch operation at the BL1B line of UVSOR Facility (Institute of Molecular Science, Okazaki, Japan, beam energy: 750 MeV) as a photon source, photoluminescence (PL) spectra from the sample before and after degradation by PDs were measured. The PL decay characteristics were measured by a single photon counting method using SR under single-bunch operation (SR duration: 0.55 ns, interval: 177 ns). Furthermore, the crystalline structure was observed by X-ray diffraction spectroscopy (XRD).

Results and Discussion

In our previous work, surface observation using an atomic force microscope shows superiority in PD resistance of NC-5 to PA [1]. Fig. 1 shows PL spectra excited by SR photons at 5.2 eV, before and after degradation by PDs. Note that the PL intensities are normalized by the height of the PL peak around 4.3 eV. The spectral shape of the rather broad PL peak around 3.0 eV differs between the samples before and after the PDs, and the difference is much clearer in PA. The decay profiles of the 3.0 eV PLs observed in NC-5 and PA before and after the PD degradation agree with the profile of an apparently similar PL peak at 3.0 eV observed in polyethylene irradiated by an ArF excimer laser. Since the PL in polyethylene originates from polyenes induced in the degradation process [2], the PLs observed in NC-5 and PA should similarly originate from polyenes. The result shown in Fig. 1 indicates that the number of polyenes induced by the PD degradation is suppressed by the effect of nanofillers. Fig. 2 shows XRD spectra obtained for NC-5 before and after the degradation by PDs. Curve (a) shows a diffraction peak around 9.5°, which indicates that Na^+ ions are present in the inter-layer regions [3]. When NC-5 was degraded by PDs, a new peak appears around 8.5° as shown in curve (b). This result suggests that the nanofillers were rearranged and piled up in parallel with their surfaces with a mutual distance around 1.0 nm. Such layered structures seem to contribute to the high durability against PDs of NC-5.

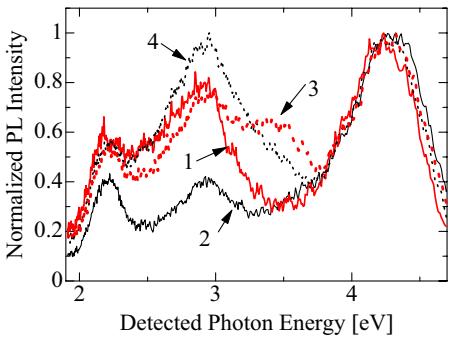

Fig. 1 PL spectra excited by SR photons at 5.2 eV. Curve 1: NC-5 before degradation, 2: PA before degradation, 3: NC-5 after degradation by PDs, 4: PA after degradation by PDs.

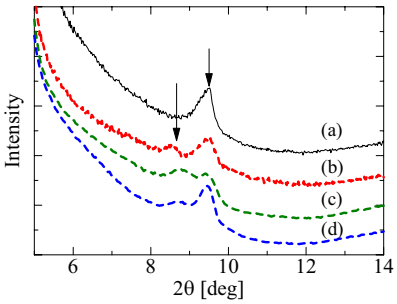

Fig. 2 XRD spectra of NC-5 before degradation (a), degraded by PDs (b), degraded by an active plasma (c), and degraded by a weak plasma (d). Since the volume of the sample differed among the samples, the intensity cannot be directly compared.

[1] M. Kozako *et al.*, IEEE Trans. Dielectr. Electr. Insul., Vol. **11**, No. 5 (2004) 833.
[2] T. Ito *et al.*, IEEJ Trans. FM, Vol. **124**, No. 7 (2004) 624.
[3] K. Yasue *et al.*, Japan Plastics, Vol. **47**, No. 6 (1996) 100 (in Japanese).

BL1B

Luminescence Properties of Tl^+ Centers Doped in KH_2PO_4

T. Fuyuki, N. Ohno

Division of Electronics and Applied Physics, Graduate School of Engineering
Osaka Electro-Communication University, Neyagawa, Osaka 572-8530, Japan.

Ferroelectric material potassium dihydrogen phosphate KH_2PO_4 (KDP) single crystals containing a small amount of thallium ions Tl^+ exhibit five characteristic polarized absorption bands A_z, A_{xy}, B_{xy}, and C_z in the ultraviolet region [1,2]. Symmetry of the local crystal field at Tl^+ ion which replaces the potassium ion is approximately S_4 in the ferroelectric phase. The observed experimental results have been qualitatively explained by taking into account the spin-orbit, crystal-field and electronic-vibrational interactions [3].

In the present study, photoluminescence and photo-excitation spectra of KDP:Tl^+ have been investigated at the BL1B station at the UVSOR facility. The optical measurements of CDP:Tl^+ have been also carried out. Single crystals of KDP and CDP containing ~ 0.02 mol% Tl^+ ions were grown by slowly cooling a saturated aqueous solution at about 60°C after several times of recrystallization.

Figure 1 shows the luminescence (green solid curve) and the excitation spectra (blue and red solid curves) of KDP:Tl^+ measured at 12 K. The broken curve in the figure is the absorption-edge spectrum of an undoped KDP for comparison [4]. A broad luminescence band excited with 5.66 eV photons is observed at 4.50 eV, showing a Gaussian lineshape and a large Stokes shift. The excitation spectra for the 4.50 eV band for polarization $E//c$ and $E \perp c$ are depicted by blue and ed solid curves, respectively. It is found that the 4.50 eV band is induced under the excitation of the A, B and C absorption bands associated with impurity Tl^+ ions [2,3]. The present excitation spectra of the 4.50 eV band indicate that the 4.50 eV is originated from the relaxed excited states of the Tl^+ ion.

Figure 2 shows the 4.50 eV luminescence spectra at temperatures between 12 and 300 K. The excitation was made with 5.66 eV photons (A band excitation). The luminescence spectra exhibit a drastic change at the ferroelectric transition temperature T_C = 123 K; the peak energy shows a high-energy shift with increasing temperature at $T \leq T_C$, and then an abrupt low-energy shift above T_C. The bandwidth has also been changed drastically at T_C. These results indicate clearly that the relaxed excited electronic states of the Tl^+ ions are strongly influenced by the ferroelectric local field due to surrounding ligand ions.

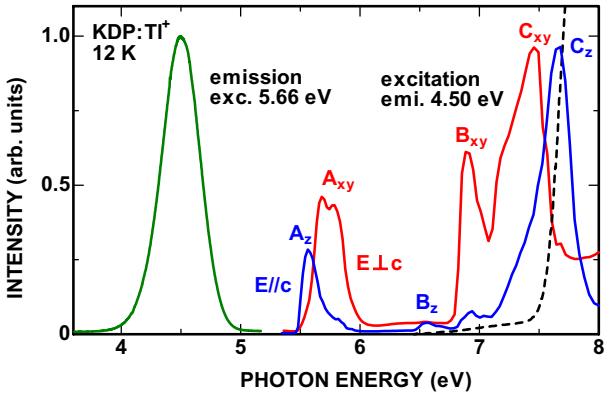

Fig. 1 Luminescence (green), excitation of the 4.50 eV band (blue and red) and absorption (broken) spectra of KDP:Tl^+ measured at 12 K.

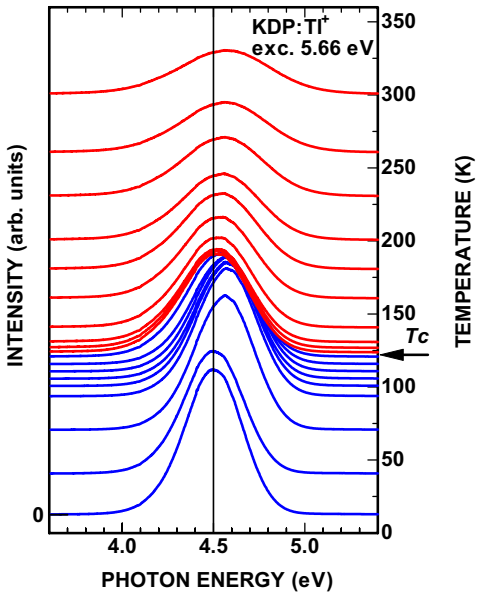

Fig. 2 Temperature dependence of the 4.50 eV luminescence spectra of KDP:Tl^+ at 12 to 300 K.

[1] I. Fujita, J. Phys. Soc. Jpn. **44** (1078) 275.
[2] I. Fujita, J. Phys. Soc. Jpn. **46** (1079) 1889.
[3] I. Fujita, Phys. Rev. B **49** (1994) 6462.
[4] T. Fuyuki and N. Ohno, UVSOR Activity Report 2003 (2004) 51.

BL1B

Luminescence of Bi^{3+} Ions Doped in $NaYF_4$

T. Hirai[1], K. Chong[1], N. Ohno[1], T. Kawai[2], S. Hashimoto[2]
[1]*Graduate School of Engineering, Osaka Electro-Communication University, Neyagawa 572-8530 Japan*
[2]*Faculty of Science, Osaka Women's University, Sakai 590-0035 Japan*

Xe dimer (Xe_2) discharge fluorescent lamps have recently attracted much attention as alternative lighting devices to conventional Hg discharge fluorescent lamps. The Xe_2 discharge generates vacuum ultraviolet (VUV) light peaking at around 172 nm. For the practical use of Xe_2 discharge fluorescent lamps, it is necessary to develop new phosphors that convert the VUV light efficiently into blue, green and red light.

Oxide phosphors have been used in the Hg discharge fluorescent lamps. In most of the oxide phosphors, the VUV light below 200 nm is little absorbed by the activators because of the absorption of the oxide hosts, so that the conversion of the VUV light is unlikely to be efficient. Most fluoride hosts, by contrast, are transparent down to ~150 nm. Thus, we expect that the fluoride phosphors are suitable for use in the Xe_2 discharge fluorescent lamps, because the VUV light generated by Xe_2 discharge (~172 nm) can directly excite the activators.

Several groups have extensively studied electronic transitions in rare earth ions doped into fluorides [1]. Some of the rare earth ions such as Eu^{3+} show absorption due to $f^n \rightarrow f^n$ (f - f) transitions in the VUV spectral region (150−200 nm). Since the absorption due to the parity-forbidden f - f transitions is weak, the conversion of the VUV light by those rare earth ions is probably inefficient.

Metal ions with s^2 electronic configurations in insulating hosts, called Tl^+-type impurity ions, exhibit strong absorption due to parity-allowed $s^2 \rightarrow sp$ transitions at the longer wavelength side of the host absorption. The strong absorption by Tl^+-type ions may lead to efficient conversion of the VUV light. However, Tl^+-type ions in fluoride hosts have been less investigated so far.

In the present study, we have investigated luminescence and excitation spectra of Bi^{3+} ions doped in $NaYF_4$ by using synchrotron radiation at the BL1B of the UVSOR facility. The Bi^{3+} ions are trivalent Tl^+-type ions that easily substitute for Y^{3+} ions in $NaYF_4$.

The right-hand side of Fig. 1 (350−600 nm) shows the luminescence spectrum of $NaYF_4$:Bi^{3+} excited at 172 nm at room temperature. One can see a broad luminescence band peaking at ~430 nm. This luminescence band is attributed to the radiative transitions from the relaxed excited states ($^3P_1$) to the ground state ($^1S_0$) in Bi^{3+} ions. On the left-hand side of Fig. 1 (100−350 nm), the excitation spectrum for the luminescence band at 430 nm is shown. Several excitation bands are observed at around 300, 250 and 200 nm. These excitation bands should arise from the transition from the ground state to some excited states given by the *sp* electronic configuration.

It is well known that Tl^+-type ions doped in alkali halide crystals with NaCl-type structure show three absorption bands originating from the intra-ionic transitions: A, B and C bands, named in sequence of decreasing wavelength. The A, B and C bands have been assigned to the transition to $^3P_1$, $^3P_0$ and $^1P_1$ states, respectively. In Bi^{3+} ions doped in Cs_2NaYCl_6, A and C bands have been observed at ~320 and 220 nm [2]. In Bi^{3+} ions in fluoride hosts, those absorption bands would shift toward the shorter wavelength side, as compared to those in chloride hosts. Accordingly, we can attribute the excitation bands at 300 and 200 nm to A and C bands. However, the origin of the strongest excitation band at 250 nm is unclear at present. Further experiments are needed to clarify the origin. Finally, it should be noted that $NaYF_4$:Bi^{3+} absorbs the VUV light generated by Xe_2 discharge (~172 nm) due to the electric dipole allowed $^1S_0 \rightarrow {}^1P_1$ transition (C absorption), and yields the blue luminescence (~430 nm).

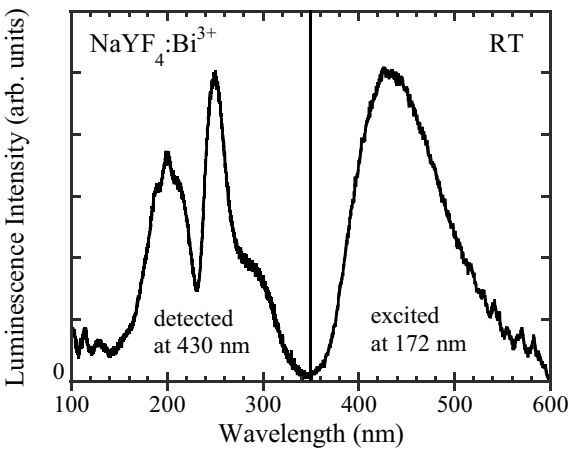

Fig. 1 Excitation (left) and luminescence (right) spectra of $NaYF_4$:Bi^{3+} at room temperature.

[1] R. T. Wegh, A. Meijerink, R-J. Lamminmäki, J. Hölsä, J. Lumin. **87-89** (2000) 1002.
[2] A. C. van der Steen, phys. stat. sol. (b) **100** (1980) 603.

BL1B

Detection of Host-Guest Complexation at the Water Surface by Photoionization Measurements

T. Ishioka, A. Harata

Department of Molecular and Material Sciences, Kyushu University, Kasugakoen 6-1, Kasuga-shi, Fukuoka 816-8680, Japan

Photocurrent has been measured at an ionophore-modified water surface by synchrotron radiation. Lower shift of photoionization threshold was observed when guest anion (phosphoric acid) was present in the aqueous solution. It is suggested that host-guest complex is formed at the water surface by hydrogen bondings.

Introduction

Threshold energy measurements of photoionization at the water surface give useful information on electric states and structures of adsorbed species [1]. Photoionization by SR light is convenient for measuring precise threshold energy by its inherent tunability in photon energy. However, it has not been fully applied to the analysis of surface reactions such as host-guest complexation at the water surface.

Host-guest complexation by hydrogen bonding is essential for molecular recognition in biological systems and it is known that interfaces plays important roles in enhancing such interactions. Air/water interface is one of such interfaces and specific hydrophobic nature has been reported by various spectroscopic measurements such as sum-frequency generation.

In this report, neutral ionophore for dihydrogen-phosphate ion is spread on anion-containing water surface and measure threshold energies for analyzing host-guest interaction that is too weak to be measured in bulk aqueous solutions.

Experimental

The monochromated synchrotron light (4-8 eV) was obtained from BL1B at the UVSOR facility and emitted from the chamber to a He-purged cell through an MgF_2 window. The emitted light was reflected on an Al mirror and vertically irradiated on the aqueous solution surface through a Cu-mesh electrode. The electrode was set at 5 mm high above the liquid surface and high voltage (500 V) was applied. The photocurrent (~ 100 fA) was measured by a picoammeter.

An ionophore optimized for dihydrogenphosphate recognition (Fig. 1) was synthesized from 2-aminoanthraquinone and dissolved in benzene at 0.2 mM. The benzene solution was spread by 10 μL on the surface of aqueous solutions containing 0.1 M anion species as acid solutions.

Results and Discussion

Used ionophore shows 1:1 complexation with dihydrogenphosphate in acetonitrile and its binding constant is estimated to be 14,000 M^{-1} by UV-VIS absorption measurements while the ionophore does not show any complexation in aqueous solutions. The difference by solvents can be explained by inhibition of host-guest complexation by hydrogen bonds with water molecules.

Photoionization threshold of the ionophore at the water surface depends which anion species is present in the bulk solution (Table 1). Compared to perchlorate and sulfate, lower shift of photoionization threshold was observed when chloride and phosphate in the solution. The trend conincides with the general affinity of anions by hydrogen bondings that is evaluated to $ClO_4^-<NO_3^-<Cl^-<H_2PO_4^-$. These results suggest that hydrogen-bonded complex is formed at the water surface.

Photoionization threshold is known to relate with standard electrochemical potential of the molecule. If we assume that the state of molecular polarization by surrounding molecules does not largely change by complexation and the difference is regarded as constant value at the water surface, the complexation constant can be evaluated by the shift of photoionization threshold. The shift of threshold energy for the complex with dihydrogenphosphate is 0.13 eV lower than the value of perchlorate and the binding constant for the ionophore in radical cation form is estimated 160 times larger than its neutral form. The enhancement factor coincides with the value in acetonitrile and the molecular environment at the water surface resembles in acetonirile.

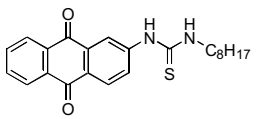

Fig. 1 Structure of synthesized inophore for dihydrogenphophate recognition.

Table 1 Measured threshold energy of the ionophore at the water surface with 0.1 M anion species in solution.

Solute	Threshold enegy / eV
None	6.03
$HClO_4$	6.12
H_2SO_4	6.13
HNO_3	6.08
HCl	6.04
H_3PO_4	5.99

[1] T. Ishioka, A. Harata, UVSOR Activity Report 2003 (2004) 62.

BL1B

Surface-Sensitive Variation of Reflection Spectra of $ZnWO_4$ in the Exciton Band Region

M. Itoh[1], N. Fujita[1], S. Takagi[1], T. Shimizu[1], M. Fujita[2], S. Oishi[1]
[1]*Faculty of Engineering, Shinshu University, Wakasato, Nagano 380-8553*
[2]*Japan Coast Guard Academy, Wakaba, Kure 737-8512*

As is well known, reflection spectra are very sensitive to the surface condition of samples. Zinc tungstate ($ZnWO_4$) is not exceptional. To our knowledge, its reflection spectrum was first measured in 1999 [1]. Since then, two research groups have reported the reflection spectra of $ZnWO_4$ [2-4]. However, there are some serious discrepancies among their results.

We have continued reflection measurements of $ZnWO_4$ at every opportunity for the past five years. The results obtained during this period are reported in the present paper.

Experiment

$ZnWO_4$ has the wolframite structure ($P2/c$). All the measurements were carried out for oriented crystals at 6 K. The SR light was incident on the (010) face with the electric vector parallel to the crystal c-axis.

Results and Discussion

Figure 1 shows three reflection spectra of $ZnWO_4$ in the 3-10 eV range. The spectrum (a) was measured for an as-grown surface of the crystal obtained from Dr. Alov (Russia). This specrum resembles those of Refs. [1,2]. The spectrum (b) was measured for an as-grown surface of the crystal grown by the flux method. The curve (c) was recorded from the same surface as that of (b) two years later, in substantial agreement with the result of Ref. [3]. One may see clear discrepany and change among the spectra (a), (b) and (c).

The crystal used for the measurement of (c) in Fig. 1 was fleshly cleaved in the air. The reflection spectrum of the cleaved surface is shown by the solid curve in Fig. 2, along with the transmission spectrum (broken curve). This reflection spectrum is similar to that of Ref. [4], although fine structures are more clearly seen here. We believe that the result of Fig. 2 is the most reliable one.

In the tungstates, the valence band is mainly built of the O 2p state and the conduction band is composed of the W 5d state. In Fig. 2, a clear peak at 4.37 eV is reasonably attributed to the lowest exciton band originating in the cationic transition, because of the sharpness and narrowness. This fact indicates that the Zn 3d and Zn 4p states contribute, to some extent, to the top of the valence band and the bottom of the conduction band, respectively. Similar hybridization of the electronic states between metal and WO_4^{2-} ions has been confirmed experimentally for $PbWO_4$ [5]. The broad band(s) at around 6.0 eV is commonly observed in the tungstates and is assigned to the O 2p→W 5d transition.

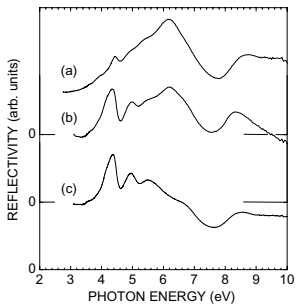

Fig. 1 Reflection spectra of $ZnWO_4$ crystals with different surface condition.

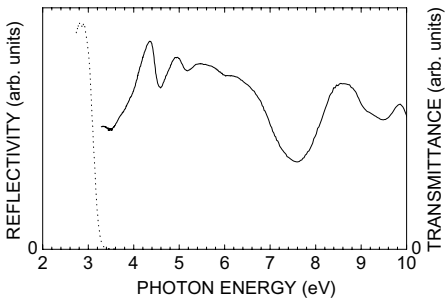

Fig. 2 Reflection (solid) and transmission (broken) spectra of a fleshly cleaved surface of $ZnWO_4$ crystal.

[1] M. Itoh *et al.*, UVSOR Activity Report 1999 (2000) 72.
[2] V. N. Kolobanov *et al.*, SCINT99, Moscow State Univ. (2000) 648.
[3] V. N. Kolobanov *et al.*, Nucl. Instrum. Methods Phys. Res. A **486** (2002) 495.
[4] V. Nagirnyi *et al.*, Nucl. Instrum. Methods Phys. Res. A **486** (2002) 395.
[5] M. Fujita *et al.*, Phys. Rev. B **65** (2002) 195105.

BL1B

Photoluminescence of Hydroxyapatite Irradiated by Ultraviolet Synchrotron Orbital Radiation Light

M. Ohta

Department of Material Science and Technology, Faculty of Engineering, Niigata University, 8050 Ikarashi 2-no-cho, Niigata 950-2181, Japan

Rare earth is used in various materials around us until now, for example phosphors, magnetic materials, catalyst, optical glass, and so on. Recently, rare earth is also useful as a contrast medium for magnetic resonance imaging, restriction enzyme, biocatalyst, and so on in fields of biochemistry, physiology, medicine, etc. However, the behavior of rare earth in the living body system remains an open question until now. It was known that rare earth ions dosed for oral administration to mouse and rat are transferred to blood vessel through the ileum and deposited its teeth and bone, which mainly consists of hydroxyapatite ($Ca_{10}(PO_4)_6(OH)_2$) [1-2]. We have found that Eu ion substituted Ba ion in Eu doped $Ba_{10}(PO_4)_6Cl_2$ phosphor, which matrix is apatite structure [3]. In this study, rare earth ion-doped hydroxyapatite samples were prepared in order to make clear the segregation mechanism of rare earth ion on teeth and bone. Their characteristics were investigated by photoluminescent property of rare earth ion-doped hydoxyapatite samples excited by ultraviolet synchrotron orbital radiation light.

Gd-doped hydroxyapatite and Yb-doped hydroxyapatite samples were prepared as follows: hydroxyapatite was soaked in $GdCl_3$ or $YbCl_3$ aqueous solution. After 72 hr, Gd-doped or Yb-doped hydroxyapatite was separated from $GdCl_3$ or $YbCl_3$ aqueous solution by filtation and then dried by using with infrared ray.The photoluminescent property of each sample exited by ultraviolet synchrotron orbital radiation light (BL1B) was detected by using with a multi-channel analyzer.

Figure 1 shows photoluminescence spectra of rare earth ion-doped hydroxyapatite samples excited by BL1B. The photoluminescent spectra of rare earth ion-doped hydroxyapatite exited by 100 nm or 150 nm had many peaks which were not ascribed to rare earth ion. These facts indicates the traps of electron and/or hole due to the defects of crystal structure exits in rare earth ion-doped hydroxyapatite, since the photoluminescent property is similar to that of self doped phosphors.

The photoluminescent spectra of Yb-doped hydroxyapatite exited by 200 nm or 250 nm had a broad peak due to charge transfer state (CTS) $\rightarrow {}^2F_{2/5}$ of Yb^{3+} [4] or due to $4f^{13}5d^1 \rightarrow 4f^{14}$ of Yb^{2+} [5]. On the other hand, that of Gd-doped one are thought to have not a peak due to Gd^{3+}. These facts indicate the existence of Yb^{3+} or Yb^{2+} as a lattice ion.

When hydroxyapatite particles were soaked in $GdCl_3$ or $YbCl_3$ aqueous solution, the amount of Gd ion deposited on the surface of hydroxyapatite particles was less than that of Yb ion. Therefore, the existence of Gd^{3+} as a lattice ion cannot be confirmed from this experiment.

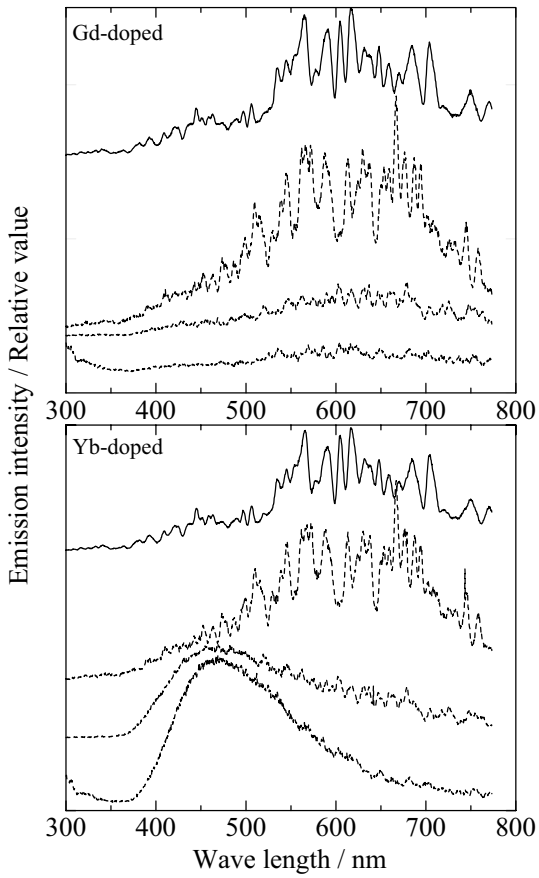

Fig. 1 Photoluminescent spectra of rare earth ion-doped hydroxyapatite samples excited by ultraviolet synchrotron orbital radiation light.

[1] S. Hirano, K. T. Suzuki, Environ. Health Perspect. **104** (Supplement 1) (1996) 85.
[2] K. Kostial, B. Kargacin, M. Lendeka, Int. J. Radiat. Biol. Relat. Stud. Phys. Chem. Med. **51** (1987) 139.
[3] M. Sato, T. Tanaka, M. Ohta, J. Electrochem. Soc. **141** (1994) 1851.
[4] F. C. Palilla, B. E. O'Reilly, V. J. Abbbruscato, J. Electrochem. Soc. **117** (1970) 87.
[5] E. Nakazawa, J. Lumin. **18/19** (1979).

BL1B

Band-Structure Design of Fluoride Complex Materials for Deep Ultraviolet Light Emitting Diode

R. E. Ouenzerfi[1], A. Quema[1], H. Murakami[1], S. Ono[1], N. Sarukura[1], T. Nishimatsu[2], N. Terakubo[2], H. Mizuseki[2], Y. Kawazoe[2], A. Yoshikawa[2], T. Fukuda[2]

[1] *Institute for Molecular Science, Okazaki 444-8585 Japan*

[2] *Tohoku University, Aoba-ku, Sendai 980-8577, Japan*

There had been continuous efforts for the development of wide-gap solid-state optical devices in the short wavelength region over these two decades. The operating wavelength is basically limited by the band gap of materials and is controlled by selecting the composition of complex materials. From this viewpoint, the most prominent candidates are fluorides. The main advantage of fluorides is their wide band gaps. Additionally, fluorides have wide-selection of complex materials, and are possible to select the band structure, band gap and lattice constant as predicted by Nishimatsu *et al.*

To determine the $Li_{(1-x)}K_xBa_{(1-y)}Mg_yF_3$ composition suitable for the design of either a light emitting diode or a laser diode; the energy gap, band structure and the lattice constants of perovskite $LiBaF_3$, $LiMgF_3$, $KBaF_3$ and $KMgF_3$ are needed. Band gap energy and band structure are determined by *ab initio* calculation within the local density approximation (LDA) as reported by Nishimatsu *et al.* [1]. The variation of both band gap energy and lattice constant as a function of the composition is investigated in analogy with a previous work on semiconductor compound lasers reported by Sasaki *et al.* This study is performed as in the case of Thompson and Woolley's work for mixed semiconductors. For $Li_{(1-x)}K_xBa_{(1-y)}Mg_yF_3$ Perovskite fluoride, the band gap energy can be written as follows :

$$E^{\Gamma,R,\Delta}_{Li_{(1-x)}K_xBa_{(1-y)}Mg_yF_3} = E^{\Gamma,R,\Delta}_{Li_{(1-x)}K_xMgF_3}\,y + E^{\Gamma,R,\Delta}_{Li_{(1-x)}K_xBaF_3}(1-y) - \frac{\alpha_{Li_{(1-x)}K_xBa_{(1-y)}Mg_yF_3}}{\sqrt{\frac{E^{\Gamma,R,\Delta}_{Li_{(1-x)}K_xMgF_3} + E^{\Gamma,R,\Delta}_{Li_{(1-x)}K_xBaF_3}}{2}}}\,y(1-y)$$

where

$$E^{\Gamma,R,\Delta}_{Li_{(1-x)}K_xBaF_3} = E^{\Gamma,R,\Delta}_{KBaF_3}\,x + E^{\Gamma,R,\Delta}_{LiBaF_3}\,x(1-x) - \frac{\alpha_{Li_{(1-x)}K_xBaF_3}}{\sqrt{\frac{E^{\Gamma,R,\Delta}_{KBaF_3} + E^{\Gamma,R,\Delta}_{LiBaF_3}}{2}}}\,x(1-x)$$

$$E^{\Gamma,R,\Delta}_{Li_{(1-x)}K_xMgF_3} = E^{\Gamma,R,\Delta}_{KMgF_3}\,x + E^{\Gamma,R,\Delta}_{LiMgF_3}\,x(1-x) - \frac{\alpha_{Li_{(1-x)}K_xMgF_3}}{\sqrt{\frac{E^{\Gamma,R,\Delta}_{KMgF_3} + E^{\Gamma,R,\Delta}_{LiMgF_3}}{2}}}\,x(1-x)$$

and

$$\alpha_{Li_{(1-x)}K_xBa_{(1-y)}Mg_yF_3} = \alpha_{KBa_{(1-y)}Mg_yF_3} + \alpha_{LiBa_{(1-y)}Mg_yF_3}(1-x)$$

Here, the energy gap sag α is assumed here to be 0.3 as proposed by Thompson and Woolley. For the lattice constant of $Li_{(1-x)}K_xBa_{(1-y)}Mg_yF_3$, we considered that the variation follows the Vegard's law. Thus,

$$a_{Li_{(1-x)}K_xBa_{(1-y)}Mg_yF_3} = a_{LiBaF_3}(1-x)(1-y) + a_{KBaF_3}\,x(1-y) + a_{LiMgF_3}(1-x)y + a_{KMgF_3}\,xy$$

The plot in Fig. 1 illustrates the quaternary chart representing the variations of R, Δ and Γ band gap valleys. The thick solid lines on the plot represent borders between either Δ and Γ domains or Γ and R ones. Compositions with equal lattice constants are represented by straight dotted lines called equi-lattice lines. From this chart, we can propose the n-$LiBaF_3$/$Li_{0.875}K_{0.125}Ba_{0.876}Mg_{0.124}F_3$/p-$LiBaF_3$ and n-$KMgF_3$/$Li_{0.870}K_{0.130}Ba_{0.847}Mg_{0.153}F_3$/p-$KMgF_3$ double-hetero structure LD emitting in around 198 nm (6.25 eV). This structure will be sufficient for LED. With appropriate cavity design, LD will be also feasible.

The LDA generally underestimates the width of band gaps. The transmission edges of $LiBaF_3$ and $KMgF_3$ single crystals are estimated down to 126.3 nm and 121.5 nm from Fig. 2. For $KMgF_3$ single crystals, an absorption dip around 130 nm might be attributable to defects of crystals. The transmission edges are defined as absorption coefficient of 20 cm^{-1}. The transmission edges of $LiBaF_3$ and $KMgF_3$ correspond to energy band gaps of 9.8 eV and 10.2 eV, respectively. The measured band gaps of $LiBaF_3$ and $KMgF_3$ are 51% and 40% higher than calculated values of 6.51 eV and 7.29 eV. From these results, there is a possibility that complex fluoride optical devises operate with shorter wavelength than that predicted by *ab initio* calculation within the LDA.

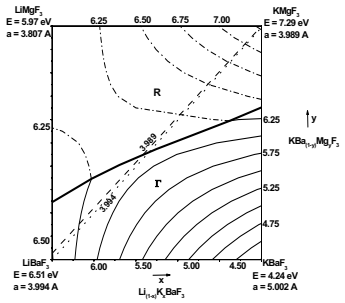

Fig. 1 Variations of band gap energy structure and lattice constants of $Li_{(1-x)}K_xBa_{(1-y)}Mg_yF_3$ with respect to composition.

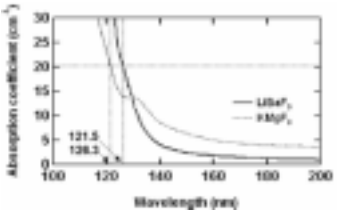

Fig. 2 Absorption coefficient of $LiBaF_3$ and $KMgF_3$ compounds in ultraviolet region

[1] T. Nishimatsu *et al.*, Jpn. J. Appl. Phys. **41** (2002) L365.

[2] R. El Ouenzerfi *et al.*, J. Appl. Phys. **96** (2004) 7655.

BL1B

Vacuum-Ultraviolet Reflectance Spectroscopy of Strongly Correlated Electron System

S. Miyasaka[1], J. Fujioka[1], Y. Tokura[1,2,3]

[1]*Department of Applied Physics, University of Tokyo, Tokyo 113-8656 Japan*

[2]*Correleted Electron Research Center (CERC), National Institute of Advanced Industrial Science and Technology (AIST), Tsukuba 305-8562 Japan*

[3]*Spin Superstructure Project (SSS), ERATO, Japan Science and Technology Agency (JST), Tsukuba 305-8562 Japan*

One of the most important characteristics for the correlated electron systems is the drastic re-construction of electronic structure over an energy scale of eV with changes of temperature, doping concentration, and/or external field. Therefore, optical reflectivity measurement over a wide energy range and the optical conductivity spectra derived from the reflectivity spectra provide us with very useful information about the strongly correlated electron systems.

In this beam time, we measured the reflectivity spectra of several transition-metal oxides, including V, Cr, Mn, Fe and Mo, for an energy range of 4 eV < E < 35 eV at room temperature using the beam line BL1B. The measured reflectivity data, together with the lower-energy data below 4 eV, were used to derive the optical conductivity spectra or dielectric function via the Kramers-Kronig analysis. As an example, the imaginary part of the dielectric function of single crystals of $La_{1-x}Sr_xVO_3$ with the several Sr concentration x, which are grown by a floating zone method, is shown in Fig. 1.

$La_{1-x}Sr_xVO_3$ is one of the classic Mott transition systems, although the single-crystal specimens necessary for detailed optics measurements have been lacking so far. The parent compound $LaVO_3$ is a Mott-Hubbard-type insulator with the V electron configuration of $3d^2$, and undergoes a magnetic transition from a paramagnetic to an antiferromagnetic state, and also a structural phase transition from orthorhombic to monoclinic follows right below the magnetic transition temperature. Sawada and co-workers have theoretically demonstrated that this compound in the monoclinic structural phase and related compound, YVO_3, have different types of orbital ordering, the alternate G-type $d_{xy}^1 d_{yz}^1 / d_{xy}^1 d_{zx}^1$ electron configuration for $LaVO_3$ and C-type for YVO_3. The carrier doping by substitution of La with Sr causes a transition from a correlated insulator to a metal around $x = 0.176$. The metal-insulator transition accompanies the structural phase transition related to the orbital order-disorder transition. To clarify the change of the electronic structure caused by the orbital-ordered Mott insulator-metal transition, we have revisited $La_{1-x}Sr_xVO_3$.

We present the spectra of the imaginary part of the dielectric function (ε_2) for $La_{1-x}Sr_xVO_3$ samples with several Sr concentrations in Fig. 1. In the spectrum of $LaVO_3$ ($x = 0$), the lowest optical transition A around 2 eV can be assigned to the optical transition across the Mott-type gap. Above the Mott gap, a much more intense optical transition B is clearly discerned. The position and intensity suggest that the transition be assigned to the charge transfer excitation from O 2*p* to V 3*d* upper Hubbard state. The transition is accompanied by another spectral structure C, which is 1 eV above the transition B. Above 7 eV, three peak structures, D, E, and F are observed. These absorption bands are assigned to the transition from O 2*p* to La 5*d* or V 4*s*/4*p* state, that from O 2*s* to V 3*d*, and that from La 5*p* to La 5*d*, respectively.

With the increase of Sr concentration x, the Mott-Hubbard gap disappears. In addition, the substitution of La with Sr changes the peak shape around 6 eV. The spectra for the insulating samples with $x = 0$ and 0.10 show double structure around 5-6 eV. This feature is caused by the ligand field splitting of 3*d* orbitals, which tends to stabilize the orbital ordering at low temperatures. In contrast, the double peak-structure is not observed in the spectra for the metallic sample with Sr concentration $x = 0.18$ and 0.26. The present results indicate that even in the high-energy region above 5 eV, the Sr doping causes the change of the spectral feature, which is related to the metal-insulator transition and perhaps to the orbital ordering.

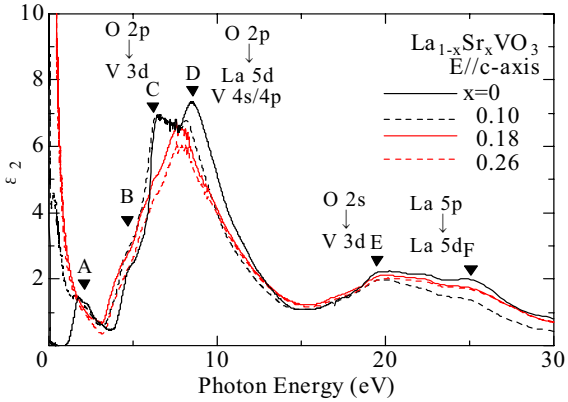

Fig. 1 The spectra of the imaginary part of the dielectric function (ε_2) for insulating samples (black curves, $x = 0$ and 0.10) and those for metallic ones (red curves, $x = 0.18$ and 0.26) in $La_{1-x}Sr_xVO_3$.

BL1B

Vacuum Ultraviolet Spectroscopy of $BaMgF_4:Ce^{3+}$ Crystals

E. Hayashi[1], K. Itoh[1], M. Yamaga[1], S. Ono[2], N. Sarukura[2]
[1]*Department of Electric and Electronic Engineering, Gifu University, Gifu 501-1193, Japan*
[2]*Institute for Molecular Science, Okazaki 444-8585, Japan*

Successful laser operation based on the $5d \rightarrow 4f$ transitions of Ce^{3+} has been reported for $LiYF_4$, $LiLuF_4$, and $LiCaAlF_6$ [1]. Recently, laser materials operating below 200 nm is required. In order to satisfy this requirement, a frequency doubling method using a nonlinear effect is useful. Ce^{3+}-doped $BaMgF_4$ (BMF) crystals attract attention as laser materials with a nonlinear effect. Recently, the BMF crystal growth and optical properties in the ultraviolet and visible range were reported [2]. In this report, we discuss the energy level of Ce^{3+} in BMF estimated from the optical spectra extended to the vacuum ultraviolet (VUV) range [3].

Figure 1 shows a unit cell of the crystal structure of $BaMgF_4$. Each octahedron consists of a central Mg^{2+} ion and six nearest-neighbour F^- ligand ions. Ba^{2+} ions are located at centers of trigonal prisms, each composed of six nearest-neighbour F^- ligand ions. Ce^{3+} ions substitute for Ba^{2+} ions. In such a configuration, the excited state of Ce^{3+} is split into E_g and T_{2g} states as shown in a lower part of Fig. 1.

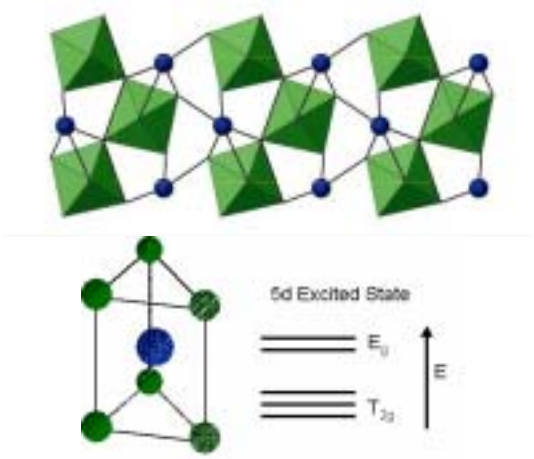

Fig. 1 A unit cell of the crystal structure of $BaMgF_4$.

Figure 2 shows absorption, excitation, and emission spectra of Ce^{3+} in BMF crystals measured at 17K in the VUV, UV and visible ranges. There are three different luminescence bands denoted by A, B, and C. Each of these luminescence bands has double peaks. The energy difference of the peak to peak is equal to the ground-state slipping between $^2F_{5/2}$ and $^2F_{7/2}$ of Ce^{3+}.

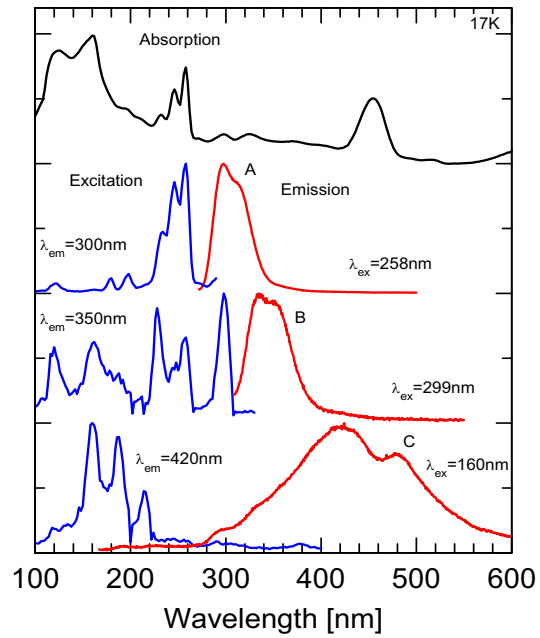

Fig. 2 Optical spectra of Ce^{3+}:$BaMgF_4$.

The excitation spectrum of the A-band luminescence consists of five broadbands at 178, 197, 233, 245, 257 nm. These bands are coincident to absorption bands. The peaks at 178/197 nm and 233/245/257 nm correspond E_g and T_{2g}, respectively as shown in Fig. 1. Similarly, the excitation spectrum of the B-band luminescence has five broadbands at 159, 228, 256, 294, 300nm. In order to identify peaks of the C-band excitation spectrum, we refer to optical spectra of Ce^{3+}:$SrMgF_4$, of which crystal structure is similar to Ce^{3+}:$BaMgF_4$. The peak of the C-band excitation spectrum are 225, 259, 298, 325, 377 nm.

These results suggest the A-band luminescence is estimated to Ce^{3+} ions which substitute for Ba^{2+} ions. The B-band luminescence is estimated to Ce^{3+} ions perturbed by Na^+ ions as charge compensators. The C-band luminescence is assigned to a complex center of Ce^{3+} and lattice defects which are different from Na^+.

[1] N. Sarukura, M. A. Dubinskii, Z. Liu, V. V. Semashko, A. N. Naumov, S.L. Korableva, R. Y. Abdulsabirov, K. Edamatsu, Y. Suzuki, T. Itoh, Y. Segawa, IEEE J. Selected Topics Quantum Electron. **1** (1995) 792.
[2] M. Yamaga, K. Hattori, N. Kodama, N. Ishizawa, M. Honda, K. Shimamura, T. Fukuda, J. Phys.: Condens. Matter **13** (2001) 10818.
[3] E. Hayashi, K. Itoh, S. Yabashi, M. Yamaga, N. Kodama, S. Ono, N. Sarukura, J. Alloys and Compounds (2005) in press.

BL1B

Temperature Dependence of Reflectivity $C_{60}F_{18}$ Single Crystals

V. G. Stankevich[1,2], A. M. Lebedev[2], N. Yu. Svechnikov[2], K. A. Menshikov[2], O. V. Boltalina[3], L. N. Sidorov[3],S.Kimura[1], M. Hasumoto[1]

[1]*UVSOR Facility, Institute for Molecular Science, Okazaki 444-8585 Japan.*

[2]*Russian Research Centre Kurchatov Institute,Kurchatov Sq.1,123182, Moscow, Russia.*

[3]*Chemistry Department, Moscow State University,119899, Moscow, Russia.*

Introduction

At present one of the most promising directions is the developing and use of new carbon nanostructures with sp^2 hybridization – fullerenes, nana tubes and thin films based on these compounds. Special interest represents investigations of fullerenes doped with different atoms leading to considerable changing of properties. Doping with halogens, in particular with fluorine, is leading to strong changes of chemical and physical properties. Additional interest for these compounds is connected with theoretical prediction [1] of significant decrease of penetration barrier for some ions and atoms through the walls of carbon nana tubes due to fluorination. Therefore, within the last few years we investigated fluorinated fullerenes $C_{60}F_{2X}$ with different amount of fluorine's.

In Ref. [2], we have investigated optical properties of different thin films based on $C_{60}F_{48}$, $C_{60}F_{36}$, $C_{60}F_{24}$ and $C_{60}F_{18}$ molecules. It was established that optical absorption edge is shifting to the higher energy region (from 1.9 eV for pure C_{60} to 4.2 eV for $C_{60}F_{48}$) due to destruction of initial π-electron subsystem of pure C_{60} and creation of new σ-orbital with C-F bonds. Besides for these compounds we have observed unusual photoluminescence temperature dependence.

All fluorofullerenes molecules are very large, with atomic masses exceeding 1000 amu and with sizes about 1 nm. These nana objects manifested very interesting molecular structures, having a spherical C_{60} skeleton, surrounded by appropriate amount of attached fluorine atoms different symmetries.

Among these, special attention should be paid to a $C_{60}F_{18}$ molecule due to a high asymmetry (Fig. 1) [3].

Fig. 1 Molecule $C_{60}F_{18}$ structure.

As seen, 18 fluorine atoms occupy only one half of a C_{60} deformed skeleton. This is leading to a high dipole moment, and theoretical estimation [3] gives the value about 10D. In principle it is possible to arrange a ferroelectric ordering at the Curie temperature T_C for ensemble of these polar molecules caused by dipole-dipole interaction. We have estimated the T_C value at first approximation. The interaction energy of two parallel identical dipoles is defined by [4]:

$$E = \frac{d^2}{R^3} \quad (1)$$

Where d – a dipole moment of molecule [D], R – a distance between two dipoles [Å], E – energy [eV]. If d = 10 D and R = 19 Å [3], the disorder temperature is found to be T_C = 112 K.

Results and discussion

Here we report first reflectivity spectra of the high quality $C_{60}F_{18}$ single crystals prepared via vacuum sublimation. Figure 2 shows the reflectivity spectra one of the rectangular plane size 100*60 microns^2 with room temperature and 50 K.

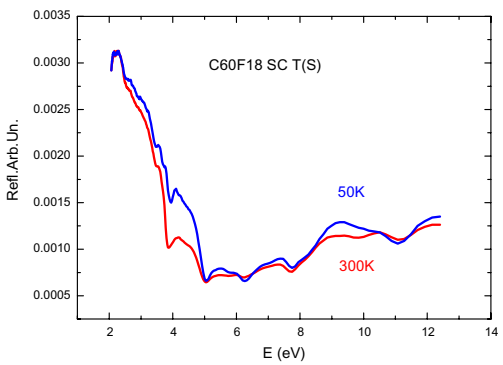

Fig. 2 Reflection spectra $C_{60}F_{18}$ single crystal.

The main changes in reflectivity are observed for the energy about 4 eV (typical for π-π* transitions) with shifting of reflection minimum to a low energy side, and for E > 8 eV for deeper electronic levels.

As a result, the observable changes of reflection spectra are demonstrating the existence of the ferroelectric phase transition; however the detail analysis and calculations are in progress now.

[1] P. V. Avramov, B. I. Yakobson, G. E. Scuceria, T. A. Romanova, IWFAC-2003 works (St. Peterburg, Russia) (2003) 22.

[2] P. V. Dudin, S. V. Amarantov, V. G. Stankevich *et al.*, Surf. Rev. Lett. **9** (2002) 1339.

[3] I. V. Goldt, O. V. Boltalina, L. N. Sidorov *et al.*, Sol. St. Sci. **4** (2002) 1395.

[4] F. Jona, D. Shirane, *Ferroelectric crystals* (Mir, Moscow) (1965) 41.

BL5B, 7B&8B1

Excitation Spectra of VIS-UV Emission in AlGaN and InAlGaN

K. Fukui[1], S. Hamada[1], S. Naoe[2], H. Hirayama[3], H. Miyake[4], K. Hiramatsu[4]
[1]*Research Center for Development of Far-Infrared Region, Fukui 910-8507, Japan*
[2]*Faculty of Engineering, Kanazawa University, Ishikawa 920-1192, Japan*
[3]*The Institute of Physical and Chemical Research, Wako 351-0198, Japan*
[4]*Faculty of Engineering, Mie University, Mie 514-8507, Japan*

AlGaN becomes a promising semiconductor optical material because of variable band gap energy from 0.8 to 6.28 eV according to composition ratio of elements. However, the photoluminescence (PL) intensity at low temperature is not sustained in increasing temperature to RT. By contrast with this, InAlGaN gives the effective rate of PL intensity at RT. Both studies of AlGaN and InAlGaN PLs are necessary to explain the mechanism of PL process in AlGaN.

All samples are made by MOCVD (MOVPE) methods. The thickness of AlGaN thin films are about 1 μm on 1 μm AlN single crystal film with sapphire substrates and those of InAlGaN thin films are about 80 nm on SiC substrates with $Al_{0.2}Ga_{0.8}N$ buffer layers. The measurements were carried out at BL7B, BL5B and BL8B1, under multi-bunches operation in the energy range from 2 to 500 eV. Same conventional 30 cm monochromator with liquid N_2 cooled CCD detector via optical fiber is used for PL measurements of all samples.

In both AlGaN and InAlGaN, PL spectra are composed of two bands. One is UV band PL (B-emission) corresponding to exciton, the other is visible (VIS) band (Y-emission) caused by lattice defects or impurities. Figs. 1 (a) and (b) show both B- and Y-emission excitation spectra of $Al_{0.34}Ga_{0.66}N$ and $In_{0.04}Al_{0.35}Ga_{0.61}N$, respectively. Intensity (vertical axis) represents the integrated intensity per excitation photon of B- or Y-emission calculated from PL spectrum at each excitation photon energy. Each spectrum is normalized for convenience. Arrows in figures represent of the peak position of B-emission and almost correspond to the band-gap energies.

Since Y-emission is caused by the recombination luminescence of electron and hole at trapping centers of defects or impurities, the excitation spectra of Y-emission are expected to give the absorption spectra of the samples originating from band-to-band transition. In fact, the excitation spectra of both AlGaN and InAlGaN Y-emission seem to be proportional to the rate of absorption of the sample. Peak-like spectral feature is only observed near band edge of AlGaN B-emission. This result suggests that the initial state of B-emission of AlGaN constructs some bound exciton states. The tail-like structures at the lower excitation energy side of InAlGaN relative to those of AlGaN probably reflects the inhomogeneous special dispersion of In element in InAlGaN alloy.

Fig. 2 shows the both excitation spectra of AlGaN and InAlGaN in the starting area of inner shell excitation. Since vertical axis (intensity) represents the integrated intensity per excitation photon, intensity increasing with increasing exciting photon energy suggests that more than one electron-hole pairs are produced during the relaxation process of an inner shell hole from core to valence band, which is known as photon multiplication.

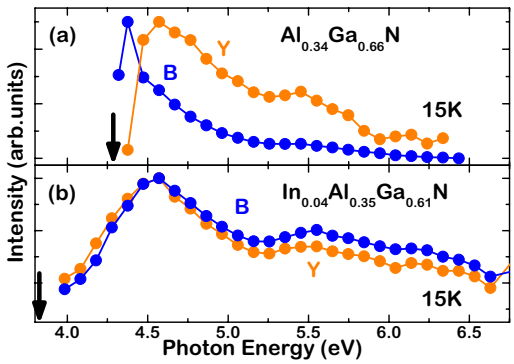

Fig. 1 Photoluminescence excitation spectra of $Al_{0.34}Ga_{0.66}N$ (a) and $In_{0.04}Al_{0.35}Ga_{0.61}N$ (b) at BL7B.

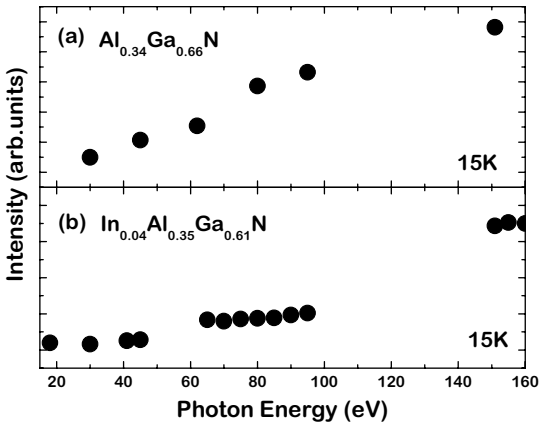

Fig. 2 Photoluminescence excitation spectra of $Al_{0.34}Ga_{0.66}N$ (a) and $In_{0.04}Al_{0.35}Ga_{0.61}N$ (b) at BL5B.

BL5B

Transmission Spectra of Amorphous Semiconductor Thin Films in the Vacuum Ultra-Violet Region

K. Hayashi

Department of Electrical and Electronic Engineering, Gifu University, Gifu 501-1193, Japan

Amorphous chalcogenide semiconductor materials, such as amorphous As_2S_3 (a-As_2S_3), amorphous As_2Se_3 (a-As_2Se_3), and amorphous Se (a-Se) etc., exhibit a variety of photoinduced phenomena. The application of these amorphous semiconductor materials to the optoelectronic devices is very much expected, because these materials are very sensitive to the light. Although a large number of studies [1-3] have been done on the photoinduced phenomena of these amorphous semiconductor materials, little is known about the details of these mechanisms. These phenomena were studied by exciting outer core electrons with the irradiation of light with the energy corresponding to the optical bandgap or sub-bandgap. The interest has been attracted for the change of the optical properties in the energy region of the visible light. Little attention has been given to photoinduced effects by exciting inner core electrons with the irradiation of higher energy photon. We are interesting for the change of the optical properties in the higher energy region. To obtain a wide knowledge of the photoinduced phenomena, it is necessary to investigate to the photoinduced effects on wide energy region. In previous reports, we reported the photoinduced change at the VUV reflection spectra of the amorphous chalcogenide semiconductor films induced by bandgap light. In present report, we report the examination on the more exact measuring method of the photoinduced change at the spectrum in the VUV region. In this report, we measured the VUV transmission spectra in amorphous chalcogenide films.

Samples used for the measurement of transmission spectrum were amorphous chalcogenide (a-As_2S_3 and a-As_2Se_3) semiconductor films. Thin films of amorphous chalcogenide semiconductor were prepared onto ultrathin collodion films by conventional evaporation technique. A typical thickness of an amorphous film was around 160 nm. The ultrathin collodion films were prepared onto stainless steel metal plates with a pinhole of the 1 mm diameter. The transmission spectrum was measured through the pinhole by a silicon photodiode. The transmission spectra in the VUV region were performed at room temperature at the BL5B beam line of the UVSOR facility of the Institute of Molecular Science. In present experiment, to eliminate the higher order light from the monochromator, an aluminum thin film was inserted between the monochromator and sample. We also monitored the spectrum of the light source by measuring the photoyield of the gold mesh. The transmission spectra were obtained by normalizing the spectra by the spectrometer system response.

Figure 1 shows the VUV transmission spectrum of a-As_2Se_3/collodion at room temperature in the wavelength region between 15 nm and 35 nm. The transmission spectrum of an aluminum filter with 100 nm film thickness supported by the metal mesh is also shown in Fig. 1. In the figure, every transmission spectrum has not been normalized by the spectroscopic system response, and that has been normalized at the maximum value of the transmitted light intensity. Two main absorption peaks of a-As_2Se_3 were observed in this region. One absorption peak around 22 nm corresponds to the 3*d* core level of Se atom. Another absorption peak around 28 nm corresponds to the 3*d* core level of As atom. These peak positions agree well with the result of the reflection spectrum [4]. In addition, it was possible to also confirm the two peaks that correspond to the core level of Se atom of $3d_{3/2}$ and $3d_{5/2}$ in present measurement. At present, it is not possible to obtain the accurate transmission spectrum, because there is a problem on effect of higher order light and reproducibility of the wavelength. It is examined in respect of these at present. The detailed experiments and analysis will be done in the next step.

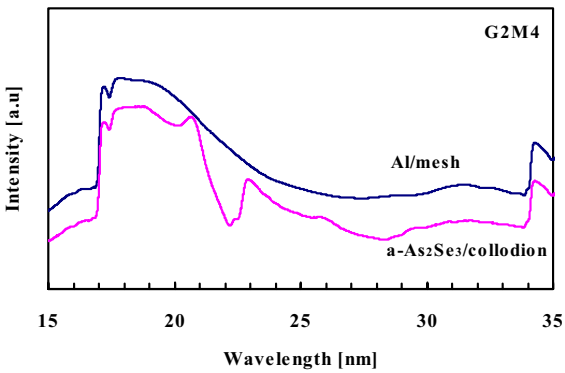

Fig. 1 Normalized transmission spectra of a-As_2Se_3/collodion and Al/mesh.

[1] Ke. Tanaka, Rev. Solid State Sci. **4** (1990) 641.
[2] K. Shimakawa, A. Kolobov, and S. R. Elliot, Adv. Phys. **44** (1995) 475.
[3] Ke. Tanaka, Encyclopedia of Nanoscience and Nanotechnology **7** (2004) 629.
[4] K. Hayashi, UVSOR Activity Report 2002 (2003) 130.

BL6B(IR)&7B

Optical Response of $CuIr_2Se_4$

L. Chen[1], T. Nanba[1], T. Matsumoto[2], S. Nagata[3]

[1]*Graduate School of Science and Technology, Kobe University, Kobe 657-8501, Japan*

[2]*National Research Institute for Metals, 1-2-1 Sengen, Tsukuba 305-0047, Japan*

[3]*Department of Materials Science and Engineering, Muroran Institute of Technology, Muroran, Hokkaido 050-8585, Japan*

The spinel compound $CuIr_2Se_4$ at atmospheric pressure is a metal at wide temperature range, but undergoes a stabilization of the insulating phase at high pressures above 3 GPa.[1,2] To study its electronic state close to the Fermi level ambient pressure, we measured the temperature dependence of optical reflectivity spectra $R(\omega)$ of polycrystalline $CuIr_2Se_4$.

Experimental

The optical reflectivity spectra $R(\omega)$ at ambient pressure was measured in the wide photon energy range from 7 meV to 30 eV in the temperature range of 8-300 K. The measurements were performed using a Fourier-transform interferometer combined with a thermal light source and synchrotron radiation source at the beam line BL6B & 7B of UVSOR. The optical conductivity $\sigma_1(\omega)$and complex dielectric function $\varepsilon_1(\omega)$ were obtained from a standard Kramers-Kronig transformation of the measured reflectivity spectrum.

Results and discussions

Figure 1 shows the temperature dependences of the R-spectra (upper panel) and σ -spectra (lower panel) of $CuIr_2Se_4$ below 25 eV. The arrow in the σ -spectra shows the direction of cooling from 300 K to 8 K. In the σ -spectra, several distinct peaks corresponding to electronic interband transitions were resolved at around 0.2, 0.8, 2.0, 4.0, 6.5 and 13 eV, together with the Drude component given by conduction electrons below 0.2 eV. The Drude component still survived even at 8 K but became narrower with cooling. The peak intensity at around 0.2 eV increased instead of the suppression of the Drude component with cooling so as to compensate the spectral weight. The peaks above 0.8 eV were almost insensitive to temperature. We fitted the σ -spectra below 3 eV with a Drude-Lorentz model and estimated the carrier densities ,for example, as 1.02 x 10^{21} cm^{-3} (300 K), 6.5 x 10^{20} cm^{-3} (80 K) and 4.6 x 10^{20} cm^{-3} (8 K). The carrier density decreases gradually with cooling but is still measurable even at 8 K.

$CuIr_2Se_4$ exhibits a broad peak structure at around 0.2 eV, which becomes distinct instead of the Drude component with cooling. The development of a low energy peak at around 0.2 eV accompanying the suppression of the Drude component suggests the precursor for the formation of the pseudo-gap state at around E_F with cooling at atmospheric pressure. Since the lattice constant of $CuIr_2Se_4$ is larger than that of $CuIr_2S_4$, temperature cooling is not sufficient to strengthen the hybridization between the 5*d* states of Ir atoms belonging to the neighboring sites ,and the Ir 5*d* and Se 4*p* states in $CuIr_2Se_4$ so as to form a clear energy gap state at around E_F. Thus, we consider that in $CuIr_2Se_4$ the weak hybridization due to the larger lattice constant might be the main reason that the metal-insulator transition does not occur at atmospheric pressure. The application of the high pressure to this compound will induce the clear opening of the energy gap state because of the increase in the hybridization by the decrease in the lattice constant. Such experiment is now on progress.

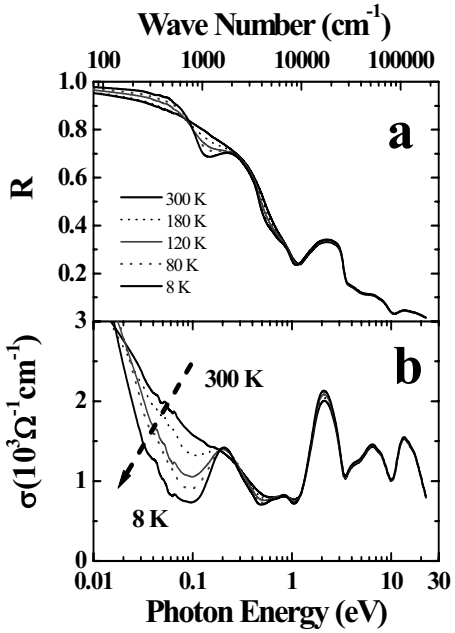

Fig. 1 Temperature dependences of (a) $R(\omega)$ and (b) $\sigma(\omega)$ -spectra from 300 K to 8 K.

[1] J. Tang, T. Furubayashhi, T. Kosaka, S. Nagata,Y. Kato and T. Matsumoto: Rev. High Pressure Sci. Technol. **6** (1997) 496.

[2] J. Tang, T. Furubayashhi, T. Kosaka, S. Nagata, Y. Kato and T. Matsumoto: Rev. High Pressure Sci. Technol. **7** (1998) 362.

BL6B(IR)

Metal-Nonmetal Transition of Bismuth Clusters

H. Ikemoto, S. Yoshida, A. Asai
Faculty of Science, Toyama University, Gofuku 3190, Toyama 930-8555, Japan

Raman-scattering measurements of clusters of bismuth exhibit a phase transition from rhombohedral Bi nanocrystalline to amorphouslike clusters depending on cluster size [1]. They also suggest that amorphous clusters are semiconducting and covalent interactions increase with decreasing size.

The Raman studies are good tools but indirect evidences for the transition. So it is very important to investigate the optical property directly to reveal the mechanism of the phase transition. In the present study we report results of optical absorption coefficients for Bi clusters.

Experimental

Bismuth of 99.999% purity was slowly deposited onto the substrates from a tungsten boat. The Bi film was discontinuous with isolated island formation. Then, KBr of 99.99% purity was deposited to cover the Bi islands. By repeating these procedures, a sample of Bi clusters isolated in an alkali-halide matrix was obtained. The size of the islands was adjusted by controlling the thickness deposited on the substrates, which was monitored with a quartz oscillator. The thickness ratio of the Bi and the matrix is about 1:20. As mentioned above the Bi clusters are formed in thin films, and samples are represented by their average thickness of the Bi thin films in this paper.

Measurements of optical absorption coefficients were performed in the energy range of 0.05 ~ 0.95 eV with the rapid-scan Michelson interferometer (Bruker, IFS-66V) at the IR beam line (BL6B) by using a KBr beam splitter. A HgCdTe detector was used.

Results and Discussion

Figure 1 presents a representative set of curves for the optical absorption coefficients of various thickness films. Several of the characteristics can be seen by examining the absorption data by itself. The absorption coefficients of the 300 nm and 10 nm thick films are close to those of bulk Bi, suggesting that these films are semimetallic. There is a noticeable change in the optical behavior between the 10 nm thick film and the 5 nm thick film. The absorption coefficients of the 5, 2 and 0.5 nm thick films are rather small compared to those of bulk Bi, indicating that those films are semiconductors.

The optical absorption coefficients for Bi thin films exhibit a phase transition from semi-metallic nanocrystalline to semiconducting amorphous clusters with decreasing the size. The semimetallic nature of rhombohedral Bi is attributed to the overlap between the back lobes of orbitals in adjacent layers, and the semiconducting nature of amorphous Bi is attributed to the loss of this overlap [2]. We suppose following mechanism of the phase transition from semi-metallic nanocrystalline to semiconducting amorphous clusters. Even if the clusters are small, the three-folded covalent bonds are similar with that of the crystalline and the layer structures are reserved. But the amorphousization of the thin films results in the disappearance of the interlayer correlation. The loss of the overlap between the orbitals in adjacent layers gives rise to the bond shrinkage and the semiconducting nature.

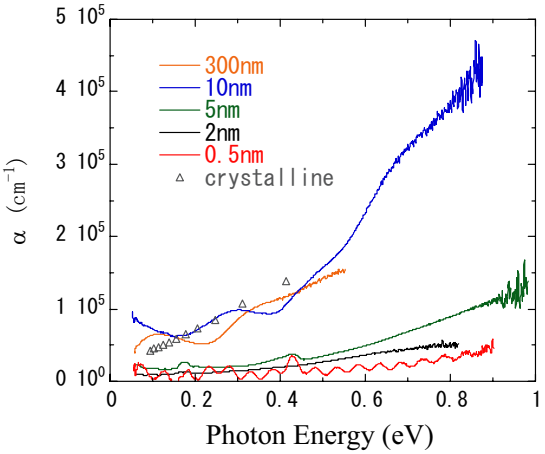

Fig. 1 Variations in optical absorption coefficients of the as-deposited Bi clusters for different thickness. Triangles denote those of polycrystalline [3].

[1] M. G. Mitch, S. J. Chase, J. Fortner, R. Q. Yu, and J. S. Lannin, Phys. Rev. Lett. **67** (1991) 875-878.
[2] N. F. Mott and E.A. Davis, *Electronic Progress in Non-Crystalline Materials*, Second Edition (Clarendon Press, Oxford, 1979) p. 413.
[3] E.V. Potapov, Soviet Phys.-JETP **20** (1965) 307.

BL6B(IR)

Terahertz Spectroscopy of a Kondo Semiconductor SmB_6

S. Kimura[1,2], S. Kunii[3]

[1]*UVSOR Facility, Institute for Molecular Scinece, Okazaki 444-8585, Japan*

[2]*Deparment of Molecular Structural Science, The Graduate University for Advanced Studies, Okazaki 444-8585, Japan*

[3]*Department of Physics, Tohoku University, Sendai 980-8577, Japan*

SmB_6, which is a typical Kondo semiconductor, has been studied over two decades. In the previous studies, two different energy gap size were proposed, one is about 5 meV and the other about 15 meV [1]. However, a recent study using higher purity samples reveals that the lower energy absorption band originates from impurities because the lower energy absorption becomes small [2]. The higher energy gap is concluded to be intrinsic and to originate from the hybridization between the localized Sm 4*f* state and the Sm 5*d* conduction band, so-called *cf* hybridization [3]. In the case of the *cf* hybridization, the electronic structure including the energy gap is rigid. However, the specific heat curve cannot be explained by the rigid band model [4]. This means that there is the temperature dependent part in the electronic structure.

On the other hand, the magnetic excitation at 14 meV grows up with decreasing temperature below 20 K observed by a neutron inelastic scattering [5]. The energy of 14 meV is similar to the energy gap observed in optical spectra. Therefore if the *cf* hybridization bands exist at the energy gap edge, the character of carriers should have the same temperature dependence. Optical reflection spectroscopy is one of good probe to investigate the character of carriers. In SmB_6 case, the signal from the thermally excited carriers appears in the terahertz region. Then we measured the temperature dependence of the reflectivity spectrum in the terahertz region.

Figure 1 (a) indicates the temperature dependence of reflectivity spectrum of SmB_6 by red marked lines. At T = 5 K, the reflectivity at $h\nu$ = 1 meV is almost constant less than unity. This indicates that the character is insulating. With increasing temperature, the spectral weight grows up from the lower energy side. The spectral weight originates from the Drude part due to thermally excited carriers. The Drude part indicates the electronic structure thermally excited area near the energy gap edge.

The fitted function using one Drude and two Lorentz functions are indicated by blue solid lines in Fig. 1 (a). The fitting functions (the parameters are not shown.) can reproduce the experimental curves well. The obtained effective electron number (N_{eff}) and relaxation time (τ) derived from the fitting parameters are shown as the function of temperature in Fig. 1 (b). N_{eff} cannot be explained by an activation type behavior [$N_{eff} \propto \exp(-2E_g / k_B T)$, where E_g is the energy gap and k_B the Boltzmann constant]. Two-state model might be assumed to explain the behavior [6]. On the other hand, τ drastically changes at 20 K. The temperature is coincident with that of the growth of the magnetic excitation at 14 meV. This means that the thermally excited carriers relates to the magnetic excitation at 14 meV.

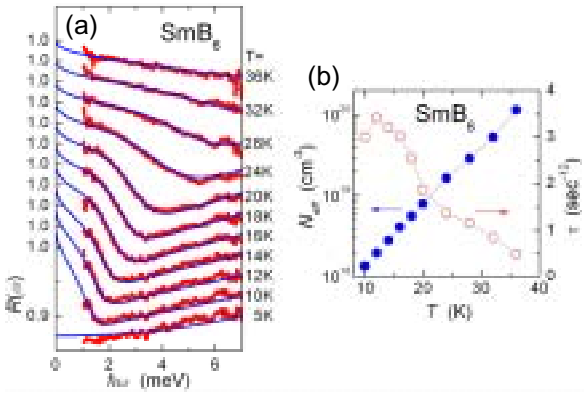

Fig. 1 (a) Temperature dependence of reflectivity spectrum of SmB_6 in the THz region (red marks) and fitting functions by the combination of a Drude and two Lorentz functions (blue lines). (b) Obtained parameters of the effective electron number (N_{eff}) and the relaxation time (τ) of the Drude function as a function of temperature.

[1] G. Travaglini and P. Wachter, Phys. Rev. B **29** (1984) 893.
[2] S. Kimura *et al.*, Phys. Rev. B **50** (1994) 1406.
[3] G. Aeppli and Z. Fisk, Comments Condens. Matter Phys. **16** (1992) 155.
[4] T. Kasuya *et al.*, *Valence Fluctuation in Solids*, (North-Holland, 1981) *p.* 215.
[5] P.A. Alekseev *et al.*, J. Phys.: Condens. Matter **7** (1995) 289.
[6] B. Gorchunov *et al.*, Phys. Rev. B **59** (1999) 1808.

BL6B(IR)

Millimeter Wave Reflection Measurements of Secondary Battery Substance $Li_xMn_2O_4$

H. Ohta[1], A. Taketani[2], H. Ishikawa[2], T. Hirano[2], T. Nanba[2], A. Hirano[3], R. Kanno[4]

[1]*Molecular Photoscience Research Center, Kobe University, 1-1 Rokkodai, Nada, Kobe 657-8501, Japan*

[2]*The Graduate School of Science and Technology, Kobe University, 1-1 Rokkodai, Nada, Kobe 657-8501, Japan*

[3]*Faculty of Engineering, Mie University, 1515 Kamihama-cho, Tsu 514-8507, Japan*

[4]*Interdisciplinary Graduate School of Science and Engineering, Tokyo Institute of technology, 4259 Nagatsuda, Midori, Yokohama 226-8502,Japan*

The Li ion secondary battery substances $LiCoO_2$ and $LiNiO_2$, are in the commercial use. $LiMn_2O_4$ is also a promising material for the Li ion secondary battery and it has attracted much attention recently. We have been studying the millimeter wave reflection measurements of $LiCoO_2$ and $LiNiO_2$ and related substances using UVSOR to investigate the dynamical properties of Li ions [1-9]. The increase of reflection is observed in the low energy region above 300 K for $LiNiO_2$ and $Li_{1-x}CoO_2$. We proposed that this increase of reflection is related to the motion of Li ion in the system but it turned out to be flat in the observed region for $LiCoO_2$ [8]. $LiMn_2O_4$ is considered as a new promising material for the positive electrode of the Li ion secondary battery from the economical point of view. Especially, a reflection measurements of $Li_xMn_2O_4$ because it corresponds to the recharge or discharge processes in the Li ion secondary battery. Therefore, we performed the millimeter wave reflection measurements of $Li_xMn_2O_4$.

The reflection measurements of $Li_xMn_2O_4$ sintered sample, in which the Li ion is extracted chemically, with a diameter of 10 mm have been performed in the spectra region from 5 to 60 cm^{-1} using the beam line BL6B of UVSOR. As $Li_{1-x}Mn_2O_4$ is very fragile, the surrounding of the sample is molded by the stycast. The low pass filter was used in order to achieve the measurement below 22 cm^{-1}. The temperature was changed from 77 to 380 K. The gold plate was used as a reference and InSb detector was used as a detector.

Figure 1 shows the reflectivity results of $Li_xMn_2O_4$. The data below 8 cm^{-1} is not reliable due to the low reflection from the reference. We can see the increase of the reflection in all temperature region from 77 to 380 K but the difference among the temperature is not clear. As $Li_{1-x}Mn_2O_4$ is very fragile, the surface condition may not be so good as other samples like $LiCoO_2$ and $LiNiO_2$. Therefore, observed increase of the reflection is intrinsic or not remains as a future problem.

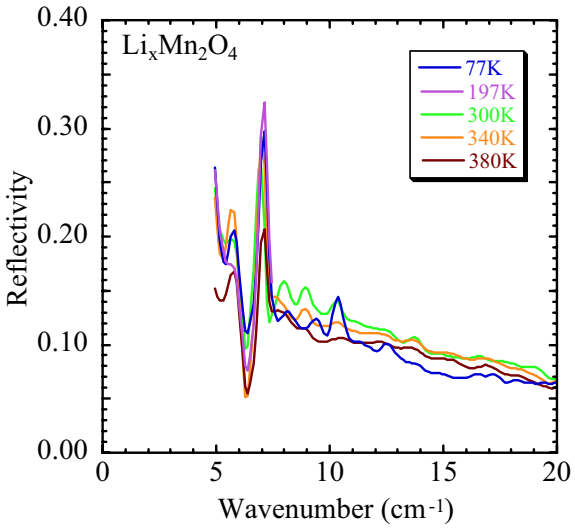

Fig. 1 Reflection spectra of $Li_xMn_2O_4$.

[1] H. Ohta *et al.*, UVSOR Activity Report 1996 (1997) 182.
[2] H. Ohta *et al.*, UVSOR Activity Report 1997 (1998) 128.
[3] H. Ohta *et al.*, UVSOR Activity Report 1998 (1999) 158.
[4] H. Ohta *et al.*, UVSOR Activity Report 1999 (2000) 93.
[5] H. Ohta *et al.*, UVSOR Activity Report 2000 (2001) 121.
[6] H. Ohta *et al.*, Jpn. J. Applied Phys. **39,** Suppl. 39-1 (2000) 409-410.
[7] H. Ohta *et al.*, UVSOR Activity Report 2001 (2002) 138.
[8] H. Ohta *et al.*, UVSOR Activity Report 2002 (2003) 142.
[9] Y. Nagasaka *et al.*, J. Phys. Chem. Solids **64** (2003) 1949-1951.

BL6B(IR)

Far-Infrared Reflectivity Measurement of YbB_{12}

H. Okamura[1], S. Kimura[2], T. Nanba[1], F. Iga[3], T. Takabatake[3]
[1]*Graduate School of Science and Technology, Kobe University, Kobe 657-8501, Japan.*
[2]*UVSOR Facility, Institute for Molecular Science, Okazaki 444-8585, Japan.*
[3]*ADSM, Hiroshima University, Higashi-Hiroshima 739-8530, Japan.*

YbB_{12} has been well known [1-3] as an example of the Kondo semiconductors [3-5]. It develops a small energy gap at the Fermi level below 80 K. The gap width in YbB_{12} has been estimated to be 12.7 meV (136 K) from electrical resistivity [2], 15 meV (180 K) from Hall effect [2], and approximately 15 meV from electronic specific heat and photoemission experiments. The gap formation mechanism in the Kondo semiconductor has been discussed extensively. In the so-called band model, the gap is regarded as a band gap resulting from the hybridization between a wide conduction (*c*) band and a flat *f*-electron band [3-5]. Previously, we reported an optical study of YbB_{12} single crystals [6]. The optical conductivity spectrum, $\sigma(\omega)$ of YbB_{12} clearly showed an energy gap formation below 80 K. The gap development involved a progressive depletion of $\sigma(\omega)$ below a shoulder at ~ 40 meV. In addition, we observed a strong mid-infrared (mIR) absorption in $\sigma(\omega)$ peaked at ~ 0.25 eV, which was also strongly *T*-dependent. However, the minimum photon energy of the previous work was limited to about 8 meV (60 cm^{-1}), and the lowest temperature was 20 K.

In this work, we have measured $\sigma(\omega)$ of YbB_{12} down to 1.3 meV (10 cm^{-1}) at 8 K. Owing to the recent upgrade of the BL6B front-end optics, both the total photon flux and the photon flux density at the sample position in the terahertz and far-infrared range (10 – 500 cm^{-1}) have become much higher [8]. In addition, a rapid-scan type Martin-Pupplet interferometer has been newly introduced at BL6B. Using this interferometer, the signal-to-noise ratio of the obtained spectra has become much higher.

Figure 1 shows the measured optical reflectivity spectra $R(\omega)$ and the optical conductivity spectra $\sigma(\omega)$. $\sigma(\omega)$ was obtained from $R(\omega)$ using the Kramers-Kronig relations. As the gap develops in $\sigma(\omega)$ with decreasing temperature below 80 K, a sharp minimum in $R(\omega)$ is observed to shift to lower energy. This minimum is the plasma edge due to the Drude response of residual free carriers. Since the carrier density decreases with gap development, the plasma edge shifts to lower energy. Previously, this shift was observed only to 40 K [6]. However, here we can observe it down to 20 K owing to the extended energy range of this work. In $\sigma(\omega)$, a clear onset of conductivity (indicated by the red arrow in Fig. 1) is observed at 15 meV at 20 and 8 K. This onset of $\sigma(\omega)$ is a direct result of the hump in $R(\omega)$, indicated by the blue arrow in Fig. 1. This onset energy of 15 meV is identified as the gap width of YbB_{12} manifested in $\sigma(\omega)$. The width of 15 meV agrees very well with those obtained by other experiments cited above. In the band model of Kondo semiconductor, there are both indirect and direct gaps in the *c-f* hybridization states near the Fermi level [4,5]. These results suggest that the gap in $\sigma(\omega)$ is due to the indirect gap. Since indirect transitions are forbidden within the first-order optical processes, it is likely that phonon-assisted transitions give rise to the appearance of indirect gap in $\sigma(\omega)$ of YbB_{12}.

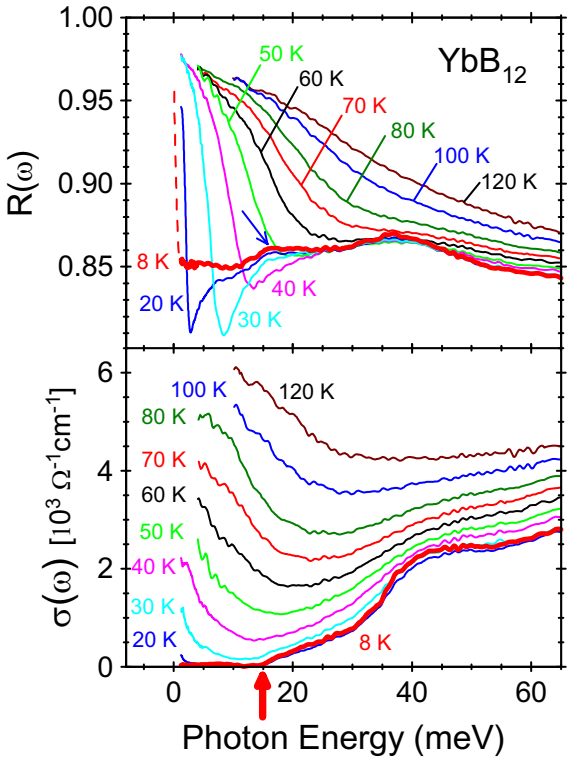

Fig. 1 (a) Reflectivity spectra $R(\omega)$ and (b) optical conductivity $\sigma(\omega)$ of YbB_{12} at various temperatures.

[1] M. Kasaya, F. Iga, K. Negishi, S. Nakai and T. Kasuya, J. Magn. Magn. Mater. **31-34** (1983) 437.
[2] F. Iga, N. Shimizu and T. Takabatake, J. Magn. Magn. Mater. **177-181** (1998) 337.
[3] T. Takabatake *et al.*, J. Magn. Magn. Mater. **177-181** (1998) 277.
[4] G. Aeppli and Z. Fisk, Comments Condens. Matter Phys. **16** (1992) 155.
[5] P. S. Riseborough, Adv. Phys. **49** (2000) 257.
[6] H. Okamura *et al.*, Phys. Rev. B **58** (1998) R7496.
[7] S. Kimura *et al.*, AIP Conf. Proc. **705** (2004) 416.

BL6B(IR)

Infrared Reflection Absorption Spectroscopy on Li-doped Alq_3

Y. Sakurai[1], S. Kimura[1], T. Yokoyama[2], K. Seki[3]
[1]*Institute for Molecular Science, Okazaki 444-8585 Japan*
[2]*Faculty of Engineering, Chiba University, Chiba 263-8522 Japan*
[3]*Research Center for Materials Science, Nagoya University 464-8602 Japan*

Tris-(8-hydroxyquinoline) aluminum (Alq_3) is most widely used as the electron transport/light emitting layer in organic light emitting diodes (OLEDs). The chemical structure of Alq_3 and its two possible geometrical isomers, meridional (C_1 symmetry) and facial (C_3 symmetry) forms are shown in Figure 1. It has been reported that the meridional isomer is the dominant species in most cases, including amorphous evaporated films.

A typical OLED consists of indium tin oxide (ITO) as the anode, on which organic thin films are sequentially deposited, with low work function metals such as Al finally deposited as the cathode. Recently, it was reported that insertion of a thin layer of an insulator such as LiF at the Al/Alq_3 interface significantly enhances electron injection. Various mechanisms for this enhancement, including the complexation between Alq_3 and Li released by the reaction between LiF and Al, have been proposed and investigated using various techniques [1,2].

Infrared Reflection Absorption Spectroscopy (IRAS) is a powerful probe for the structure and chemistry of the surface and interface. Though IR spectrum below 1000 cm^{-1} is expected to be significantly change by interaction between metal and Alq_3, it is difficult to obtain IRAS spectrum of this region using a globar source. In this paper, we report the IRAS spectra of pristine and Li-doped Alq_3 measured using synchrotron radiation (SR) source.

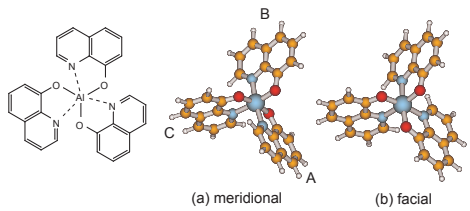

Fig. 1 The chemical structure and geometrical isomers of Alq_3.

Experiments including the sample preparation and measurement were performed in an ultrahigh vacuum chamber. Alq_3 was supplied by Nippon Steel Chemical. Ag film was deposited on Si (100) substrate from a Knudsen cell. Alq_3 film was prepared by vacuum evaporation onto this Ag film kept at room temperature. The thickness of Alq_3 film was monitored using a quartz microbalance. Lithium was deposited on the Alq_3 films from a SAES getter source. IRAS spectra were measured at BL6B of UVSOR. The spectra were obtained with SR light through a KRS-5 window and at an angle of incidence of 80° relative to surface normal. The reflected light was detected with an MCT detector.

Figure 2 shows the IRAS spectra of Alq_3 film of 20 nm thickness before and after lithium evaporation. After Li evaporation, the observed spectra show the following changes. Intensity of IR bands at 1500 and 1389 cm^{-1} becomes weak, new band appears at 520 cm^{-1}, broad bands appear around 1535-1570 and 1250-1300 cm^{-1}, band at 1471 cm^{-1} becomes broader. These changes in the region between 1000 and 1800cm^{-1} are similar to those in the case of K deposition on Alq_3 [3]. The appearance of new band at 520 cm^{-1} was newly detected by using SR source.

Figure 2 also indicates theoretically simulated spectrum of Li-Alq_3 complex in the meridional isomer by DFT calculation with B3LYP functional and 6-31G(d) basis set. The geometry optimization was carried out starting from a geometry similar to that reported by Curioni and Andreoni [4]. In the meridional isomer, the Li atom lies between ligands A and B. The simulated spectrum agrees well with the observed IRAS spectrum. The spectrum of Li-Alq_3 complex in the facial isomer is expected to be more simple and very different from that of meridional isomer because of its symmetry (Li atom is on the threefold symmetry axis) [4].

Since significant changes of IRAS spectrum are expected in the region between 300 and 500 cm^{-1} by the DFT calculation, more information will be obtained by IRAS measurement in the far-IR region.

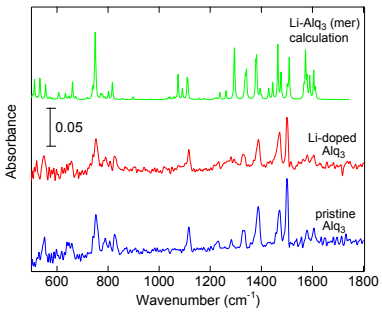

Fig. 2 IRAS spectra of pristine and Li-doped Alq_3 and theoretically simulated IR spectrum of the meridional Li-Alq_3 complex.

[1] M. G. Mason *et al.*, J. Appl. Phys. **89** (2001) 2756.
[2] P. He *et al.*, Appl. Phys. Lett. **82** (2003) 3218.
[3] Y. Sakurai *et al.*, J. Appl. Phys. **96** (2004) 5534.
[4] A. Curioni and W. Andreoni, J. Am. Chem. Soc. **121** (1999) 8216.

BL7B

Optical Spectra and Electronic Structure of Calcium Fluorapatite

M. Kitaura[1], S. Oishi[2], M. Oda[3], Y. Chikama[3], H. Nakagawa[3]
[1]*Fukui National College of Technology, Sabae 916-8507 Japan*
[2]*Dept. of Environmental Science and Technology, Shinshu University, Nagano 380-8553 Japan*
[3]*Dept. of Electrical and Electronics Engineering, Fukui University, Fukui 910-8507 Japan*

Calcium hydroxyapatite $Ca_5(PO_4)_3OH$ is of great potential for applications in medical science, because of its biocompatibility. One of the peculiar properties of this material is the ability that incorporates various cations and anions as constituents [1]. This property comes from its crystal structure, in which calcium ion and hydroxide ions are easily replaced by foreign cations and anions, respectively. Actually, it is well known that the replacement of hydroxide ions by fluorine ions causes a preventive action in the occurrence of dental cavities. The purpose of this study is to understand the fluorination effect of calcium hydroxyapatite in the viewpoint of electronic structure. In this work, the spectra of absorption and reflectivity in calcium fluorapatite $Ca_5(PO_4)_3F$ grown from KF flux [2] have been measured at 9 K using a 3-m normal incidence monochromator at BL7B.

Results and Discussion

The spectra are shown in Fig. 1. As indicated by a broken curve, the absorption edge is located around 6.01 eV. The lowest energy reflectivity peak appears at 9.51 eV. This peak accompanies a shoulder structure in the low energy side. They could not be clearly separated by varying the polarization of excitation light. Several peaks are observed in the energy range of 10-20 eV.

The electronic structure of calcium flourapatite was calculated by the DV-Xα method. The method has successfully applied for understanding of the electronic structure in organic and inorganic crystals. The detail of this method has been described in ref. [3]. Figure 2 shows the energy level diagram of a $Ca_{21}(PO_4)_{18}F_{30}$ cluster embedded in the crystal lattice. The valence band is primarily composed of the 2*p* orbitals of oxygen. The 2*p* orbitals of fluorine also includes in the upper valence band. The shallow core states are made of the 2*s* orbitals of oxygen. On the other hand, the conduction band is complicated as compared to the valence band. The bottom of the conduction band is dominated by the 4*s* orbitals of calcium. The band gap energy is estimated to be 9.47 eV.

From the calculated results, the electronic transition from the valence state of O 2*p* to the conduction state of Ca 4*s* is expected in the region near the fundamental gap, because this type of the transition is of allowed type. Therefore, we assign the 9.51 eV peak to the O 2*p* → Ca 4*s* transition. A dip is located at 10.04 eV in the high-energy side of the 9.51 eV peak. The energy is in good agreement with the calculated band gap energy, so the dip is probably regarded as an indication of the band gap position.

Our experimental results can be almost explained by the electronic structure of the model cluster mentioned here. We further continue several investigations for a detailed understanding of the electronic structure of calcium fluorapatite and calcium hydoxyapatite. On this basis, the changes in the charge density and bond overlap population by the fluorination effect will be cleared.

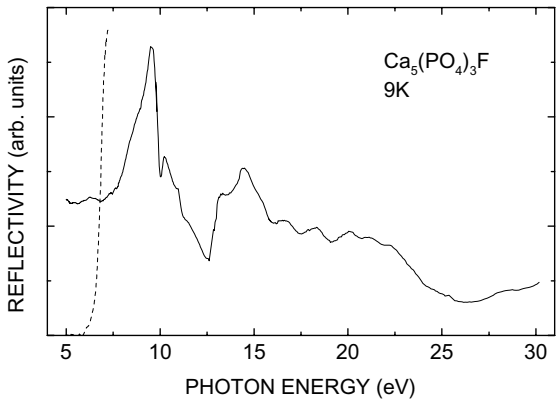

Fig. 1 Reflectivitiy (solid curve) and absorption (broken curve) spectra of calcium fluorapatite at 9 K.

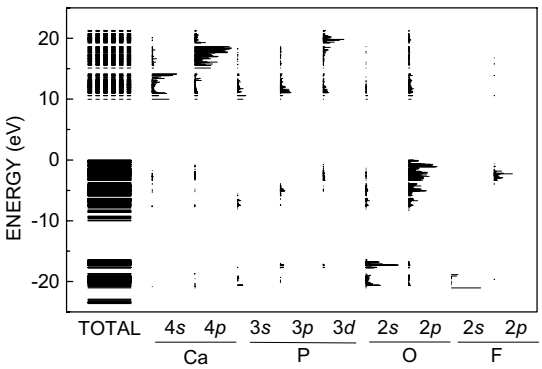

Fig. 2 Energy level diagram of a $Ca_{21}(PO_4)_{18}F_{30}$ model cluster embedded in the crystal lattice of calcium fluorapatite.

[1] For example, J. C. Rendon-Angeles, K. Yanagisawa, N. Ishizawa and S. Oishi, J. Solid State Chem. **151** (2000) 65.
[2] S. Oishi and T. Kamiya, J. Chem. Soc. Jpn. (1994) 800 (in Japanese).
[3] H. Adachi, M. Tsukada and C. Satoko, J. Phys. Soc. Jpn. **45** (1978) 875.

BL7B

Vacuum UV Reflectivity Spectroscopy of PZT and LNO

J. Mistrik[1], T. Yamaguchi[1], N. Dai[2], M. Shimizu[3]

[1]*Research Institute of Electronics, Shizuoka University, Hamamatsu 432-8013 Japan*

[2]*National Laboratory of Infrared Physics, Shanghai Institute of Technical Physics, Chinese Academy of Sciences, Shanghai 200083 China*

[3]*Division of Electronic Materials and Devices, Department of Electrical Engineering and Computer Sciences, Graduate School of Engineering, University of Hyogo, Himeji 671-2201 Japan*

Perovskite-type oxides $Pb(ZrTi)O_3$ (PZT) and $LaNiO_3$ (LNO) are interesting materials for both applied and fundamental research. In spite of this, there are only a few papers devoted to its optical properties. Recently we have reported spectroscopic ellipsometry studies on LNO and PZT thin films performed in visible and near UV spectral regions [1,2]. Our further effort is focused on the development of a new dispersion model for these materials based on parameterization of the joint density of the electronic states in the vicinity of the valence and conduction bands [3,4]. Therefore, our beam time was used to record the UV and vacuum UV reflectivity spectra of PZT and LNO samples.

Polycrystalline PZT films were deposited by sol-gel and MOCVD on LNO/Pt/Ti/SiO_2/Si seed structure and platinized Si substrates Pt/SiO_2/Si respectively. Thin monocrystalline PZT film was grown by MOCVD on SRO/STO substrate. For the study of LNO reflectivity the seed structure for PZT films, LNO/Pt/Ti/SiO_2/Si, was used.

Selected spectral range (6 - 25eV) from UVSOR synchrotron radiation was scanned by the 3-m normal incidence monochromator (beam line 7B). Two monochromator gratings G2 (600 l/mm) and G1 (1200 l/mm) and LiF filter were used to cover the studied spectral range. Incident and reflected light intensity was measured in room temperature by a Si photodiode. Angle of incidence was less then 15 deg.

Fig. 1 presents selected reflectivity spectra of sol-gel deposited polycrystalline PZT and LNO films. Reflectivity in the visible and near UV spectral ranges was carried out by spectrophotometer PerkinElmer Lambda 45 and these data were used as a reference to adjust the absolute reflectivity values of UV and vacuum UV ranges. The spectral features up to about 5 eV come from the light interference in PZT and LNO films which thickness is 217 nm and 96 nm, respectively. Obtained reflectivity spectra are typical for transition metal oxide compounds with perovskite-type structure [5]. Detailed discussion of PZT and LNO electronic structure demand the knowledge of their electronic permittivity spectra and their parameterization by joint density of electronic states. This will be done in forthcoming paper.

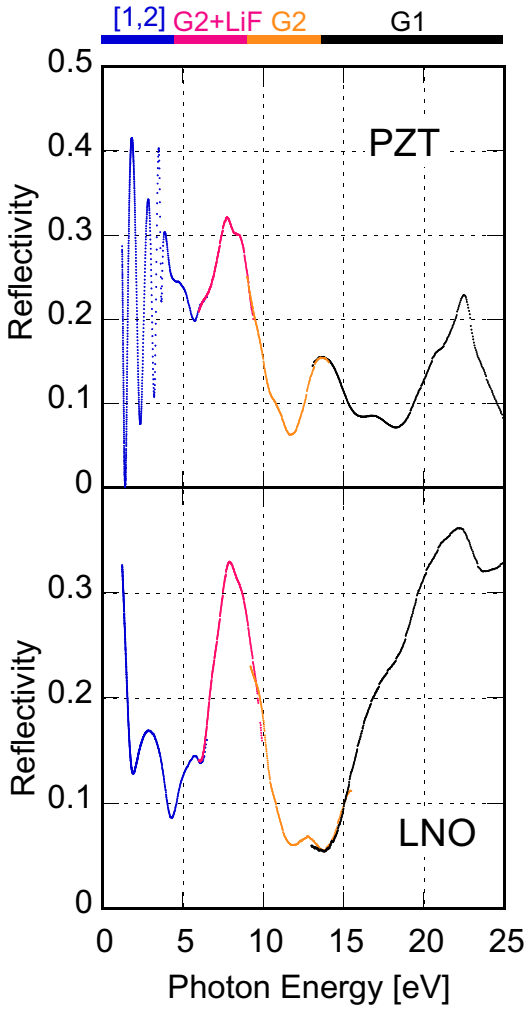

Fig. 1 Reflectivity spectra of PZT and LNO films

[1] D. Franta, I. Ohlidal, J. Mistrik, T. Yamaguchi, G. J. Hu, and N. Dai, App. Surf. Sci. **244** (2005) 338-342.

[2] J. Mistrik, T. Yamaguchi, D. Franta, I. Ohlidal, G. J. Hu, N. Dai, App. Surf. Sci. **244** (2005) 431-434.

[3] D. Franta, B. Negulescu, L. Thomas, P. R. Dahoo, M. Guyot, I. Ohlidal, J. Mistrik, and T. Yamaguchi, App. Surf. Sci. **244** (2005) 426-430.

[4] D. Franta, I. Ohlidal, M. Frumar, J. Jedelsky, App. Surf. Sci. **212-213** (2003) 116-121.

[5] T. Arima, and Y. Tokura, J. Phys. Soc. Jap. **64** (1995) 2488-2501.

BL7B

VUV Absorption Spectroscopy of SiO_2 Thin Film

K. Nakagawa, H. Mikami, T. Ishikawa, Y. Shiraishi,
A. Ejiri, H. Matsumoto, S. Matsumoto
School of Science & Technology, Meiji University, Kawasaki 214-8571 Japan

Absorption spectrum of silicon dioxide (SiO_2) thin film was studied in the VUV region with synchrotron radiation. Refractive index and extinction coefficient were carried out from Kramers-Kronig transformation using absolute values of absorption coefficients obtained from the experiment. It is necessary for accurate simulation to know absorption coefficients in higher photon energy region. On the basis of optical property of SiO_2, absorption spectrum in UV–VUV region is particularly important because of high band gap energy. Reflection spectrum of SiO_2 had been report by Philipp *et al.* [1], but the absorption spectrum of SiO_2 has not been studied. We report the absorption spectrum and optical constants n and κ of SiO_2 thin film up to 30 eV.

Experimental

The SiO_2 thin film was prepared by RF magnetron sputtering method. The SiO_2 plate with 99.99% purity was used as a target and the sputtering was carried out in argon gas under a total pressure of 0.8 Pa. The film was sputtered onto thin substrate of collodion at room temperature and the incident RF power of 100 W. The film thickness was about 15 nm.

The absorption spectrum of SiO_2 thin film was measured in the vacuum ultraviolet region up to 30 eV with the 3-m normal incident monochromator (grating: G1 and G2) at BL7B of UVSOR-II. And silicon photodiode sensor was used as a detector for the transmission light.

Results and Discussion

Figure 1 shows absorption coefficient of SiO_2 thin film at room temperature. The peaks are named as indicated in the figures for convenience. Five peaks named as A, B, C, D and E were observed at about 10.5 eV, 11.9 eV, 14.1 eV, 17.6 eV and 21.0 eV, respectively. One can see that peaks A, B, and C (below 15 eV) were characteristic sharp structure. Similar peaks have been found at the near position in the reflectance spectra of crystalline SiO_2 and fused SiO_2 reported by Philipp [1].

The optical constants were evaluated by the Kramers-Kronig analysis. Figure 2 shows the refractive index n and the extinction coefficient κ of SiO_2 thin film obtained by the Kramers-Kronig analysis from the absorption spectrum with experimental data. Refractive index and extinction coefficient obtained from experiment were measured with ellipsometer in the range from 1.5 eV to 5.0 eV. Comparing theoretical value and experimental value of optical constants, both values were good agreed with each other.

We calculate energy levels of SiO_2 by the DV-Xα molecular orbital method. From the results of calculation, the valence band (VB) is almost composed of the O 2*p* orbital, which consists of two parts, lower part and higher part. And the lowest conduction band (CB) is composed of mixed orbital of Si 3*s*, Si 3*p* and Si 3*d*. It is found that the higher VB is very tight structure. Therefore, the sharp peaks in the region of near the fundamental absorption gap may be the transition from O 2*p* to mixed orbital of 3*s*, 3*p* and 3*d* in Si.

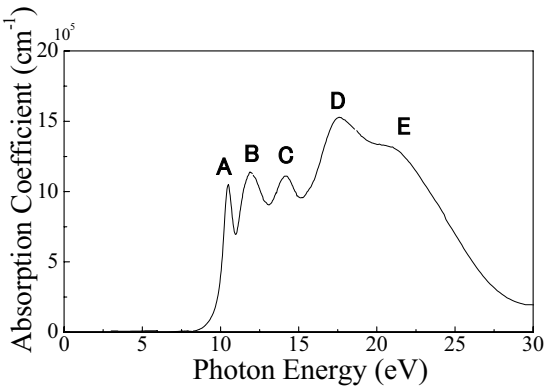

Fig. 1 Absorption spectrum of SiO_2 thin film in the region from 3 to 30 eV at room temperature.

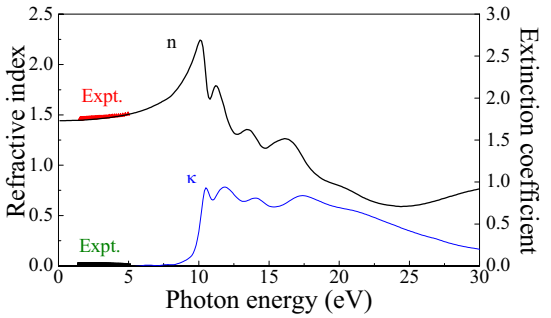

Fig. 2 Refractive index n and extinction coefficient κ spectra of SiO_2 thin film obtained by Kramers-Kronig analysis from the absorption spectrum.

[1] H. R. Philipp, Solid. State. Commun. **4** (1966) 73.